Simulation of the ionization wave discharges: a direct comparison between the fluid model and E–FISH measurements

Yifei Zhu[1,2], Xiancong Chen[2], Yun Wu[1,2], Jinbo Hao[3], Xiaoguang Ma[5], Pengfei Lu[3,4], Pierre Tardiveau[6]

[1] Institute of Aero-engine, School of Mechanical Engineering, Xian Jiaotong University, Xian 710049, People's Republic of China
[2] Science and Technology of Plasma Dynamics Laboratory, Airforce Engineering University, Xi'an 710038, People's Republic of China
[3] School of Science, Xian University of Architecture and Technology, Xian 710055, Shaanxi, People's Republic of China
[4] State Key Laboratory of Information Photonics and Optical Communications, Beijing University of Posts and Telecommunications, Beijing 100876, People's Republic of China
[5] School of Physics and Optoelectronic Engineering, Ludong University, Yantai 264025, Shandong, Peoples Republic of China
[6] LPGP, CNRS, Univ. Paris-Sud, Universit Paris-Saclay, F-91405, Orsay, France

E-mail: wuyun1223@126.com, yifei.zhu.plasma@gmail.com

Abstract.

Numerical modeling and experimental measurements are developing in parallel, for a long period there is a resolution gap in between, making it hard to conduct a direct comparison. In this work we numerically studied the diffusive ionization wave and fast ionization wave discharge experiments with recently published E–FISH data using a classical fluid model. The pressure–E/N range of the drift diffusion approximation and the pressure-grid range of the local field/mean energy approximation for the fluid model are proposed. The three–terms Helmholtz photo–ionization model is generalized with parameters given for N_2, O_2, CO_2 and air. The capabilities of the classical fluid method in modeling the inception, propagation and channel breakdown stages are studied. The calculated electric field evolution of the ionization are compared with E–FISH measurements in discharge development stage and gap-closing stage, the influence of the electrode shape and predefined electron density on the streamer morphology, the long existing inception problem of the ionization waves are discussed in detail. Within the application range of the classical fluid model, a good agreement can be achieved between calculation and measurements.

PACS numbers: 82.33, 52.25, 52.65

Keywords: plasma modeling, fluid model, fast ionization wave, streamer discharge, E–FISH

1. Introduction

Low temperature plasma discharges operating at moderate and high pressure (much larger than tens of mbar) have received increasing attention in recent years, both in academic research groups and in industries for their ability to produce active species in well-controlled environments at low energy cost. These discharges are found in a growing list of successful practical applications such as ozone generation [1], polymer processing [2], excitation of laser and excimer lamps [3], pollution control [4], combustion and ignition [5], medical treatment [6], aerodynamic flow control [7], and thin film coating [8].

A simple way to generate low temperature plasma at moderate and high pressure is to use electrodes at high-voltage separated by a gaseous gap. However, the originally cold plasma could rapidly become a high-conducting junction that evolves into a thermal spark [9, 10] where heavy species tend to be in equilibrium with the electrons at a few tens of thousands degrees Kelvin, leading to huge amount of energy consumptions and destruction of chemical species. One way to prevent this equilibrium of temperature between heavy species and electrons is to use Nanosecond Pulsed Discharges (NPD), which are usually produced by a short duration and high peak voltage on the electrodes. The NPD is also one of the most powerful tool for diagnostics of fundamental processes of plasma sources due to its excellent reproducibility and flexibility in tunning parameters.

The demand of probing nanosecond pulsed plasma sources at moderate and high pressures for deeper insight and effective control is increasing during the past tens of years. Electrical discharges at such pressures are featured by small mean free path of electrons compared to the characteristic length scales of the discharge [11], thus can be described by taking the first or second moment of Boltzmann equation with the drift-diffusion approximation, which is called the fluid method or the fluid model.

The fluid method has been successfully implemented in different codes [12–15] and commercial softwares for simulating e.g. streamer discharges [16,17], plasma jets [17,18] and dielectric barrier discharges [19, 20] in nanoseconds time scale. Compared to particle simulations the fluid method is much more computational efficient and flexible in treating chemical reaction systems and multi-physics coupling problems.

For a long period, the comparison between simulation and measurements are limited to time integrated morphology of some specific emitting only species [21] or current values with noises due to the influence of impedance mismatching, displacement current and electromagnetic interference [22]. Other comparisons focus on code-to-code comparison [23]. There exists a quite big "resolution gap" both in space and time between numerical simulations and experimental measurements, some physics happened in extreme conditions (e.g. very high electric field , ultrafast rising voltage) may be missing when the fluid model fails to predict and the measurements cannot capture.

Some laser based, non–intrusive diagnostic method have been developed to detect the electric field in the discharge plasma, e.g. Four–wave–mixing Coherent Anti-Stokes Raman Scattering (CARS) spectroscopy [24,25]. Later the Electric field induced second

harmonic (E–FISH) generation technique is proposed [26–28], the E–FISH technique has attracted quite a large attention due to its simplicity in implementation and its excellent temporal (sub–nanosecond) and spatial (sub–millimeter) resolution. The measurement based on E–FISH have bee conducted in various configurations, e.g. dielectric barrier discharges, surface discharges and plasma jets [29–32]. As electric field is one of the key parameters determining the transport and reaction rates concerning electrons, the use of E–FISH technique makes it possible to conduct direct comparison with simulations in a higher resolution. However, it has to be mentioned that, the field strengths measured by EFISH could also be in error, due to the mechanism of signal generation when focused laser beams are used [33], or with the nature of the calibration approach employed [34]. These issues will probably not affect the shape of the electric field temporal evolution profile significantly, but the quantitative values could be inaccurate.

The E-FISH technique, although in development, has attracted a wide attention from the community due to its simplicity and satisfactory accuracy shown in existing publications. Meanwhile, the direct comparison between simulation and E-FISH results, especially in extreme conditions and non-quasi-one-dimensional conditions is rarely seen. In this work, we make a comparison between fluid modeling and recent E–FISH measurements. Two typical nanosecond pulsed plasma sources consisting of extreme conditions with detailed measurements are considered: the dielectric constraint fast ionization wave at moderate pressure with very high field [35–37], and the volumetric pin–to–plane diffusive discharge at atmospheric pressure under extremely fast voltage rising slope [38,39]. The fluid model is implemented in the validated *PASSKEy* (PArallel Streamer Solver with KinEtics) code [20, 40–42]. The aim is to study the capabilities of the classical fluid model in presence of extreme conditions in nanosecond pulsed plasma discharges, and to reduce the resolution gap between modeling and measurements with analysis or solutions for the discrepancies.

2. Typical ionization wave discharges with extreme conditions

The ionization waves can be categorized based on their relation between bounding dielectrics with three representatives: the free volumetric streamers generated between two metals; the fast ionization wave discharges generated in a capillary tube; the surface ionization waves generated in surface dielectric barrier discharge configurations, bounded by a dielectric layer on one side.

2.1. Diffusive ionization wave discharge in atmospheric pressure

The diffusive ionization wave discharge studied in this work is triggered in atmospheric pressure by a voltage pulse with extremely fast rising rate (10–35 kV/ns) and 40–86 kV amplitude [38, 39]. The voltage pulse is applied in a pin–to–plane configuration with pin curvature radius of 50–100μm and gap distance of 16 mm. The ultrafast voltage increasing rate leads to the formation of an unique conical discharge shape with radius

comparable to the gaseous gap distance, or the so–called diffusive ionization wave.

There exists a few simulations of the diffusive volumetric ionization wave. Early studies of the discharge dynamics and morphology can be found in Ref [21, 43, 44], a large conical structure is reproduced, agreeing well with the experiments. Recently, the electric field evolution is studied qualitatively using simplified geometry and voltage profile with higher mesh resolutions [45], the influence of the voltage rising time and plateau voltage is studied.

In this work, the geometry and voltage shapes used in the simulation are exactly the same with the experiments in Ref [38], see Figure 4 in section 4.1, a direct comparison with the measurements in both the streamer propagation and the conduction stages are conducted.

2.2. Fast ionization wave discharge in moderate pressure

The fast ionization waves (FIW) considered in this work are initiated in moderated pressures (27 and 40 mbar) by a voltage pulse with fast rising rate (10 kV/ns) and 20 kV amplitude [35, 37]. The voltage pulse is applied on a pin–pin configuration constraint in a capillary tube of 80 mm in length and R=0.75/10 mm in radius. One of the pin is connected with the voltage generator while another is floated. A grounded metal shield is connected to the cable and put around the capillary tube. The FIW is featured by extremely high E/N ($>$ 1000 Td for 10 mm radius and 10000 Td for 0.75 mm radius, close to or exceeding the application limit of the drift–diffusion fluid model) in the ionization head and high specific energy deposition ($>$ 0.1 eV/mol) in the conductive stage, posing challenges on both transport and kinetics solutions.

Numerical modeling of FIW via global chemistry code, 1D model based on radial approximation [35, 36, 46, 47]/axial simplification or self-consistent 2D model have been conducted to study the species evolution and kinetics at different SED. Impressive 2D modeling of FIW via hybrid code *nonPDPSIM* in air at 27 mbar for the R=0.75 mm case can be found in [48] using a simplified voltage profile, the measured discharge dynamics and current are compared. Ref [49] numerically studied the streamer and FIW mode of nanosecond capillary discharges in air in a shorter tube (2 cm), the influence of SED on the temporal-spatial evolution of e and $N_2(C^3\Pi_u)$ was discussed for flexible control of kinetics.

The calculation of nitrogen FIW using exactly the same geometry and voltage profiles with experiments (27 mbar, R=0.75 mm) has been conducted recently [42], the basic electrical features and the influence of photo–ionizations and kinetics on the distribution of the species have been studied, but a comparison with the electric field is not available due to lacking of E–FISH data. In this work, we will not repeat the discussions in Ref [42], but will discuss it together with the newly calculated case (40 mbar, R=10 mm) that has been measured by the E–FISH technique in Ref [37].

There is another extreme condition challenging the fluid model: the extremely fast non-equilibrium to equilibrium transition [50, 51] of surface ionization waves at

elevated pressures. At elevated pressures and high voltages, the nanosecond pulsed surface discharge transformed from the "quasi-uniform" streamer mode [7, 20] to the "filamentary" mode with tens of bright filaments appeared from the HV edge and developed in the direction perpendicular to the HV edge. This phenomenon was first observed for negative polarity nSDBD in air [52], and later was found as a general feature for various molecular gases and mixtures containing molecular gases both for positive and negative polarity [53–55]. Space and time resolved optical emission measurements on surface filaments show that the transition to filamentary mode was accompanied by the appearance of intense continuous radiation and broad atomic lines [56], the electron density was characterized by high absolute values 10^{18}–10^{19} cm^{-3} and long decay 10–20 ns in the afterglow. The mechanism of the streamer–to–filament transition hasn't been fully understood thus was not fully implemented in the 2D model, but we will still discuss in the next section the application ranges of the fluid model together with this condition.

3. The plasma fluid model and approximations

The plasma fluid model can be derived taking the first and second moment of the Boltzmann equation. A set of approximations are used to close the equations system. In this section we analyze the equations trying to draw an application range of the fluid model with certain approximations. The numerical implements for the gap closing stage and the non-oxygen containing photo–ionization source are also discussed.

3.1. Description equations of species

The zeroth and first moment of the Boltzmann equation leads to the continuity equation, momentum and energy conservation equation:

$$\frac{\partial n}{\partial t} + \nabla \cdot \mathbf{\Gamma} = S \tag{1}$$

$$\frac{\partial \boldsymbol{u}}{\partial t} + (\boldsymbol{u} \cdot \nabla)\boldsymbol{u} = -\frac{\nabla P}{nm} + \frac{F}{m} - \nu \boldsymbol{u} \tag{2}$$

$$\frac{\partial n_\epsilon}{\partial t} + eE \cdot \mathbf{\Gamma} + \nabla \cdot \mathbf{\Gamma}_{\boldsymbol{\epsilon}} = S_\epsilon \tag{3}$$

where $\mathbf{\Gamma} = n\boldsymbol{u}$ is mean flux of particles, S denotes the source term for particles due to collisions, respectively. In this equation there are two unknown variables, number density n and velocity vector $\boldsymbol{u}$. m is the particle mass, F is the force and ν the collision frequency. The isotropic pressure P can be represented as $P = nk_bT$. $n_\epsilon = 3nk_bT/2$.

To close above set of equations, one has to truncate the moment series of the Boltzmann equation at a finite stage by a set of approximations, leading to the so called drift-diffusion (DD) fluid model. In the following section the approximations and application range are analyzed.

3.2. Approximations and the application ranges

To truncate the moment of Boltzmann equation at the first moment, a simplification of the moment balance equation 2 can be done.

First, the particle flow velocity becomes stationary in time scale of $\tau = \nu^{-1}$. If τ is shorter than the propagation time scale τ_s of streamers studied in our cases, the first term of equation 2 can be considered as 0:

$$\frac{\partial \boldsymbol{u}}{\partial t} \sim 0 \tag{4}$$

Second, if $|(\boldsymbol{u}\cdot\nabla)\boldsymbol{u}| \ll \nu\boldsymbol{u}$, which is common in high pressure plasma discharge, both terms of the left hand side of equation 2 can be neglected, and one obtains:

$$\boldsymbol{u} = -\frac{\nabla P}{nm\nu} + \frac{\boldsymbol{F}}{m\nu} \tag{5}$$

Substitute $P = nk_bT$ into above equations, the well-known drift-diffusion approximation is achieved [57]:

$$\boldsymbol{u} = -\frac{k_bT}{m\nu}\frac{\nabla n}{n} + \frac{\boldsymbol{F}}{m\nu} = -D\frac{\nabla n}{n} + \mu\frac{\boldsymbol{F}}{q} \tag{6}$$

or in flux form:

$$\boldsymbol{\Gamma} = n\boldsymbol{u} = -D\nabla n + \mu\boldsymbol{E}n \tag{7}$$

where D and μ are the diffusion coefficient and mobility of particles, respectively. Similarly one can write the energy flux $\boldsymbol{\Gamma_\epsilon}$ for the equation 3 as:

$$\boldsymbol{\Gamma_\epsilon} = n_\epsilon\boldsymbol{u} = -D_\epsilon\nabla n_\epsilon + \mu_\epsilon\boldsymbol{E}n_\epsilon \tag{8}$$

where D_ϵ and μ_ϵ are the diffusion coefficient and mobility of mean electron energy.

As it was mentioned above, the drift-diffusion approximation is based on two assumptions: (1) inertial has much smaller influence than collisions, $|(\boldsymbol{u}\cdot\nabla)\boldsymbol{u}| \ll \nu\boldsymbol{u}$ and (2) the characteristic time scale of momentum transfer is shorter than the case time scale, $\tau < \tau_s$. It is interesting to take electron (the fastest particle in a plasma system) in air mixture to make an estimation of the range of electric field and pressure in which these two assumptions are valid.

For assumption (1), $|(\boldsymbol{u}\cdot\nabla)\boldsymbol{u}| \ll \nu\boldsymbol{u}$ can be further simplified as:

$$|(\boldsymbol{u}\cdot\nabla)\boldsymbol{u}| = \alpha u^2 = \nu_i u \ll \nu u => \nu_i \ll \nu \tag{9}$$

where α is the first Townsend coefficient, and ν_i is ionization frequency. The variation of ν_i and ν with respect of E/N for air can be plot in Figure 1(a), which shows that, the accuracy of drift-diffusion approximation will drop starting from 2000 Td, if we consider $10\cdot\nu_i < \nu$ as equivalent to $\nu_i \ll \nu$.

For assumption (2), a contour plot of τ with respect to different pressure and E/N can be used to find the validate boundary of drift-diffusion approximation, by finding the domain where characteristic time scale of streamer propagation, $\tau_s = 10^{-9}s$ is larger than τ. In Figure 1(b), the given limitations based on assumption (1) and (2) are plot

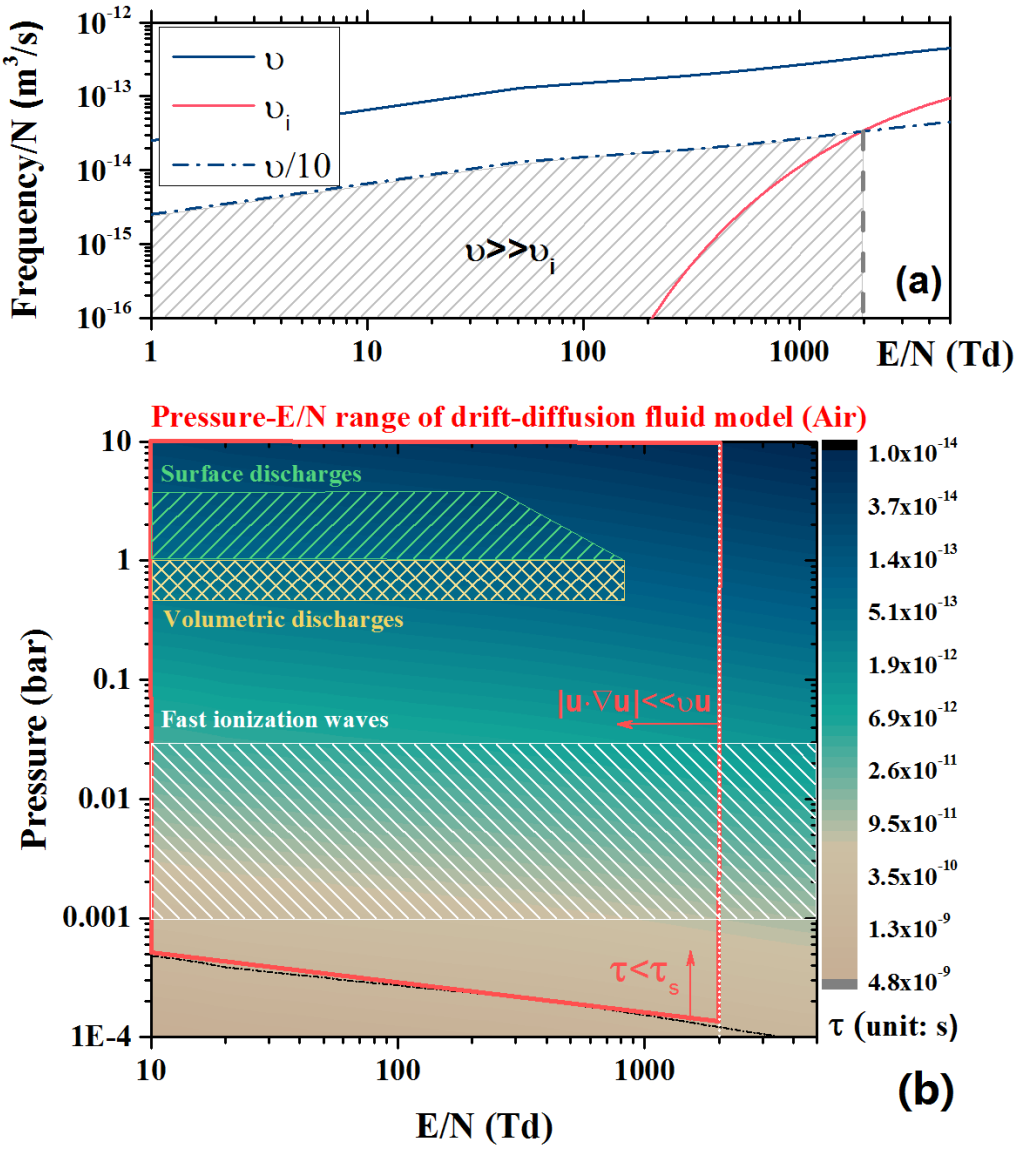

Figure 1. (a) Variation of effective momentum transfer frequency ν and ionization frequency ν_i in dry air. Region covered with gray dense lines indicate validate E/N domain for drift-diffusion approximation. (b) Characteristic time scale of effective momentum transfer in dry air at 300K in Pressure-E/N plot. Shadow region denotes the ranges of typical plasma sources. The red lines indicate the estimated boundary of drift-diffusion approximation, out of which the accuracy will drop. The data for the figures are calculated using BOLSIG+ code [58].

together as a dash dot line and a dash line. The pressure-E/N domain above dash dot line and left of dash dot line is the valid region in which the accuracy of drift-diffusion approximation is ensured. The estimation of ν, ν_i and τ mentioned above are made with the help of BOLSIG+ code.

We plotted three typical types of discharges in Figure 1, which will be discussed in detail in following sections. In general the surface discharges and volumetric streamers

can be well modeled with the drift–diffusion approximation. For the fast ionization waves, the drift–diffusion model may lose accuracy at the ionization head where the electric field reaches 10^4 Td at moderate pressures.

Solving equations 1,3,7 and 8 require the information of the electron transport coefficients and rate coefficients. These parameters can be obtained by solving the Boltzmann's equation based on the two-terms approximation [58] assuming local equilibrium of electrons is achieved instantaneously in time in response to the electric field (local field approximation, LFA) or the mean electron energy (local mean enery approximation, LMEA).

The validity of LFA have been discussed in various publications [59–62], deviations from the LFA were studied for negative streamers in nitrogen at atmospheric pressure [61] by means of a comparison between 1D fluid and particle models. By taking into account the nonlocal effects, all of these authors found an increase of the ionization in the streamer head, resulting increase of the electric field and a small increase of the streamer velocity. The discrepancies given by LFA are far smaller than an order of magnitude. For example, Ref [61] found a relative difference between the fluid and the particle models of 10% to 20% in the ionization level behind the streamer front for homogeneous applied electric fields of 50 kV/cm and 100 kV/cm, respectively. For practical accuracy, one can obtain the main streamer characteristics by a fluid model [59], especially for positive ionization waves.

More accuracy can be achieved based on LMEA [63, 64]. When the discharge interacts with dielectrics, the role of LMEA on the resolution and accuracy becomes visible. In the near-wall region where plasma bottom side is close to the dielectric surface, LFA may lead to overestimation of ionizations. Ref [65] has mentioned that, the electrons may move against the E-field force due to the strong diffusion associated with the high concentration gradient and enter into the region of a strong E-field. In this region, the predicted ionization source based on LFA is very high and the electron-ion density grows dramatically. The real ionization source cannot be so high, because the electrons lose their energy moving against the E-field force and cannot ionize gas molecules so effectively. This problem will become non-negligible in case of moderate pressure discharges when the sheath region has to be resolved. Ref [65] used a corrected ionization electron source to overcome this problem, a more general method would be incorporating an additional energy continuity equation.

To have a quantitative view on the application range of LFA/LMEA, we make a simple estimation based on the effect of "electron cooled by field". Assuming there is a sheath region where electron density n_e will drop from n_{emax} to 0 in length L_{sheath}, and the diffusion flux is larger than convection within this region:

$$D_e \nabla n_e > \mu n_e E \tag{10}$$

let n_{eavg} be the average electron density within the sheath, assuming Einstein

relationship $D_e = \mu T_e$, then above equation can be simplified as:

$$\mu T_{es} \frac{n_{\text{emax}}}{L_{\text{sheath}}} > \mu E_s n_{\text{eavg}}, \rightarrow L_{\text{sheath}} < \frac{T_{es}}{E_s} \frac{n_{\text{emax}}}{n_{\text{eavg}}} \tag{11}$$

where T_{es} and E_s are the electron temperature and electric field in the sheath region. If one consider $n_{\text{emax}} = 2n_{\text{eavg}}$, then the length of $L_{\text{sheath}} < 2T_{es}/E_s$ can be considered as the limit length, below which the behavior of plasma can not be resolved by LFA. One can make an estimation of the criteria length L_{sheath} with respect to pressure variations using BOLSIG+, see the blue line in Figure 2. If the mesh grid size is smaller than L_{sheath} (the light blue region below the blue line) then LMEA should be used, otherwise LFA is recommended for higher computational efficiency (the light red region above the blue line).

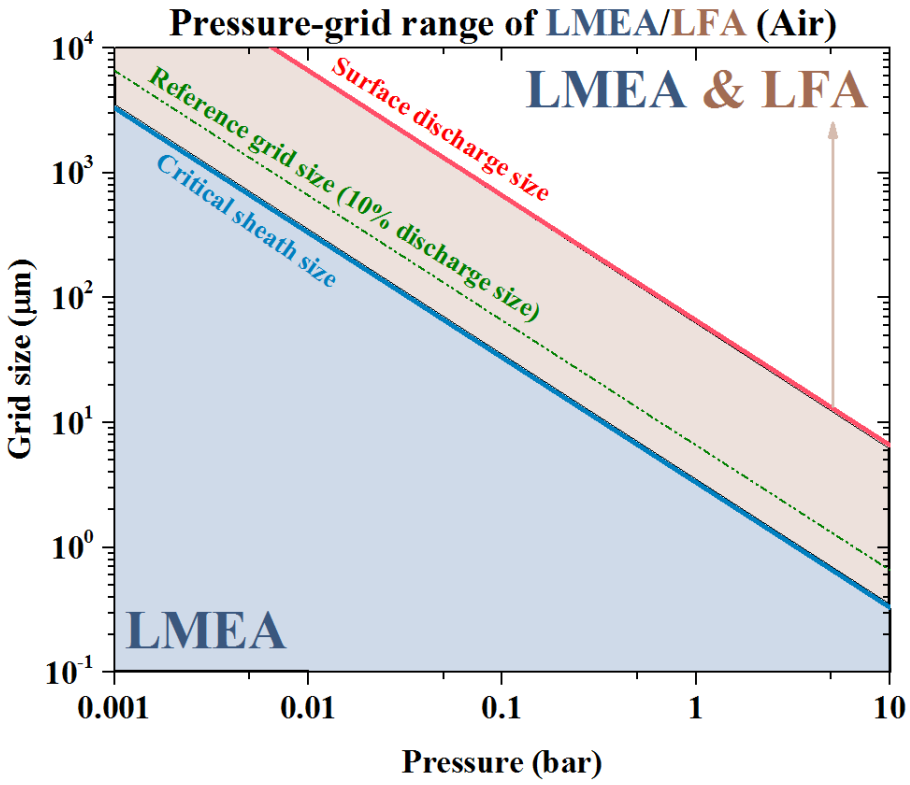

Figure 2. The characteristic sizes of the surface discharges (red), grids (green) and sheath (blue). If the model grid size falls in the light blue region (below the blue line) then LMEA (or a corrected electron flux boundary [66]) is prefered to avoid the "electron cooled by field" problem, otherwise both LMEA and LFA provides satisfactory results.

The upper range of LFA is limited by the characteristic size of the discharge channel. By fitting previous calculations and measurements of surface discharges [20, 66, 67], we can write the streamer thickness at different pressures as $h_d[\mu\text{m}] = 65.9/p[\text{bar}]$, see the red line in Figure 2. To resolve the streamer at least 10 mesh grids have to be distributed

in the plasma region thus we add a green line as a reference of the basic grid size. The green line lies in the LFA region, indicating that in general LFA is satisfactory for modeling surface discharges [20, 40]. However there are special cases: (i) the discharge is bounded in limited region, e.g. the fast ionization wave operated in a tube with inner radius of 750 μm [48, 49]; (ii) the fine structure of plasma–solid interaction region is of interest [66, 68]. Notes that in Ref [66] the accuracy of the plasma–dielectric sheath region is assured by introducing an correction term to the LFA scheme instead of using LMEA.

As LMEA gives higher flexibility in modeling nanosecond plasma discharges with extreme conditions, in this work all the calculations are conducted based on LMEA. The negative ionization waves are not studied, as the role of fast electrons vital for negative discharges have been discussed in detail in a series of publications [19, 61, 69, 70] and cannot be resolved by a pure fluid model. All the cases studied in this work are cathode directed discharges for the convenience of direct comparison with measurements.

3.3. Coupling equations

The drift–diffusion–reaction equations of species and electron energy have to be coupled with the information of electric field, kinetics and photo–ionization source terms.

The electric field is obtained from Poisson's equation:

$$\nabla(\varepsilon_0\varepsilon_r\nabla\Phi) = -\rho - \rho_c \tag{12}$$

$$\boldsymbol{E} = -\nabla\Phi, \rho = \sum_{i=1}^{N_{\mathrm{ch}}} q_i n_i \tag{13}$$

$$\frac{\partial\rho_c}{\partial t} = \sum_{j=1}^{N_{\mathrm{ch}}} q_j[-\nabla\cdot\boldsymbol{\Gamma_j}] \tag{14}$$

where n_i, q_i, $\boldsymbol{\Gamma_i}$ are the number density, charge and flux of each species i, respectively. Φ is the electric potential, $\boldsymbol{E}$ the electric field, ε_0 is the vacuum permittivity, ε_r the relative permittivity, ρ_c the dielectric surface charge density. N_{total} and N_{ch} are the number of all species and charged species, respectively.

The right hand side of equation (1) includes the kinetics source term S_i and photo–ionization source term S_{ph}, $S = S_i + S_{\mathrm{ph}}$. The kinetics source term includes production and loss of species due to gas phase reactions, the selection of kinetics and corresponding reaction rates depends on the research target, a developing list of reaction scheme describing the propagation dynamics and fast gas heating in air/nitrogen for 2D modeling can be found in previous publications [40–42, 71]. The source term of electron energy equation (3) represents the power lost by electrons in collisions can be calculated from the BOLSIG+ code [58, 72].

The photo–ionization source terms S_{ph} are vital for positive discharges in providing seed electrons. A well defined model consisting of three-exponential Helmholtz equations [73, 74] have been proposed to calculate the photo–ionization source term

of $N_2 : O_2$ mixtures, a table of fitting coefficients are provided based on the measured photo–ionization functions. However, the classical three-exponential Helmholtz model assumes that photoelectrons comes only from the ionization of O_2 molecules by VUV-radiation of N_2 in $b^1\Pi_u$, $b'^1\Sigma_u^+$, $c'^1_4\Sigma_u^+$ states [75], thus the model and corresponding parameters are valid only for $N_2 : O_2$ mixtures.

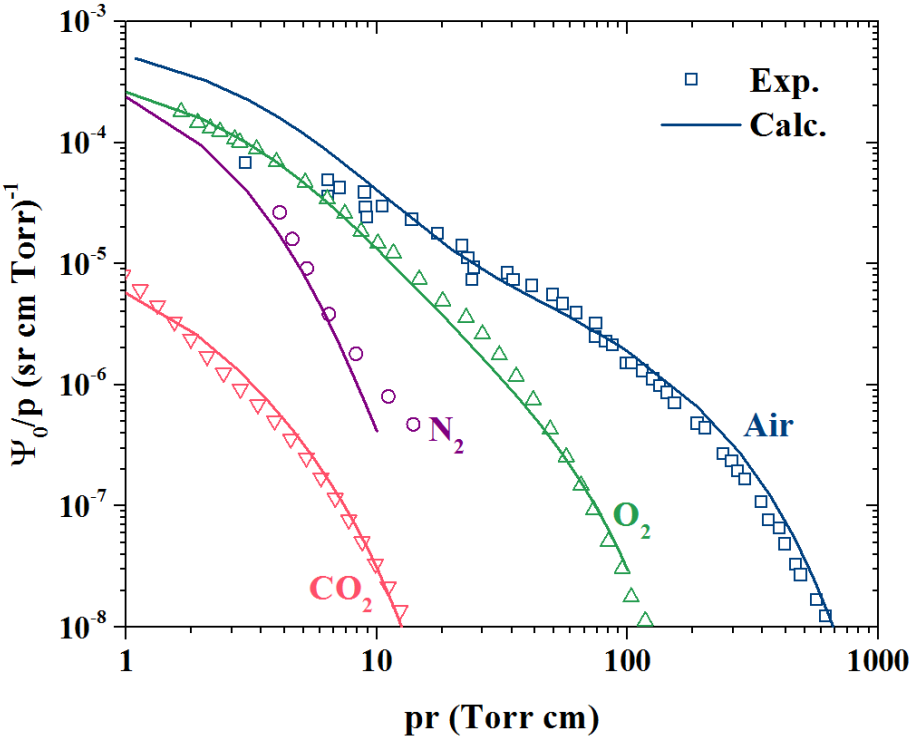

Figure 3. Photo–ionization functions Ψ_0/p of air, O_2, N_2, CO_2. The hollow symbols and solid lines represent experimental values extracted from Ref [76] and calculated values by the PHOTOPiC package, respectively. Note that the calculated results from PHOTOPiC are multiplied with $(p + p_q)/p_q$ to compare with the measurements conducted at low pressures, where p is the operating pressure, p_q is the quenching pressure of the ionized gas.

In order to calculate the photo–ionization source term in a more general way, we generalize the classical three-exponential Helmholtz model by replacing the partial pressure of oxygen molecules p_{O_2} with total pressure p:

$$S_{\text{ph}}(\vec{r}) = \sum_j S^j_{\text{ph}}(\vec{r}) \tag{15}$$

$$\nabla^2 S^j_{\text{ph}}(\vec{r}) - (\lambda_j p)^2 S^j_{\text{ph}}(\vec{r}) = -A_j p^2 \frac{p_q}{p + p_q} I(\vec{r}) \tag{16}$$

$$\frac{\Psi_0(r)}{p} = (pr) \sum_j A_j \mathrm{e}^{-\lambda_j pr} \tag{17}$$

$$\frac{\Psi_0(r)}{p} = \frac{1}{4\pi} \frac{\omega}{\alpha_{\text{eff}}} \frac{\int_{\lambda_{\min}}^{\lambda_{\max}} \xi_\lambda (\mu_\lambda/p) \exp((-\mu_\lambda/p) pr) I^0_\lambda \mathrm{d}\lambda}{\int_{\lambda_{\min}}^{\lambda_{\max}} I^0_\lambda \mathrm{d}\lambda} \tag{18}$$

Table 1. Fitting parameters for the extended three terms Helmholtz photoionization model

Parameters	N_2	O_2	**Air**	CO_2
$A_1(\mathrm{cm^{-2}Torr^{-2}})$	6.646×10^{-2}	1.939×10^{-4}	1.207×10^{-3}	3.036×10^{-4}
A_2	1.3580	1.037×10^{-3}	1.301×10^{-6}	6.599×10^{-5}
A_3	-1.4165	8.235×10^{-6}	3.928×10^{-4}	9.536×10^{-6}
$\lambda_1(\mathrm{cm^{-1}Torr^{-1}})$	1.31210	0.6774	1.419	13.7256
λ_2	1.5238	1.9053	4.093×10^{-2}	3.3875
λ_3	1.5097	0.1977	4.855×10^{-1}	1.0527
pr **range**$(\mathrm{Torr \cdot cm})$	1–10	1–25.11	1–100	1–5.6

where λ_j and A_j $(j = 1, 2, 3)$ are fitting parameters for equation (17). p_q is the quenching pressure of the emitting gas, p is gas pressure, $I(\vec{r})$ is the ionization source rate, $\Psi_0(r)/p$ the photo–ionization functions as pr, ω the excitation coefficient of emitting states, α_{eff} the effective Townsend coefficient, $(\lambda_{\mathrm{min}}, \lambda_{\mathrm{max}})$ the spectral range of radiation, ξ_λ and μ_λ are the spectrally resolved photo–ionization yield and absorption coefficient, respectively, I^0_λ is the spectral density of ionizing radiation.

With the generalized three-exponential Helmholtz model, the partial pressure of a specific gas is no longer needed, it is possible to calculate photo–ionization source term of pure/multi-species (any ratio) gas discharges if a valid photo–ionization function is available for parameters fitting. The photo–ionization function can be obtained by direct measurements or by calculation [76]. A free online toolbox PHOTOPiC is developed and used for this aim. Using the product of spectrum emission intensity, the photo–ionization yield and the absorption coefficients as the input to PHOTOPiC, the photo–ionization functions Ψ_0/p of air, O_2, N_2, CO_2 is well reproduced [77], see Figure 3. The 6 fitting parameters of the extended three-terms Helmholtz model for different gas are summarized in Table 1 based on the calculated photo–ionization functions in Figure 3.

3.4. Boundary conditions

The boundary conditions of Poisson's equation and photo–ionization equations have been illustrated in detail in previous publications [20, 40, 41], the main idea is to draw a large computational domain, set Neumann conditions on the boundaries far from the plasma discharge region, and set Dirichlet conditions on metals with specific voltages.

The boundary conditions of continuity equations vary in different works [66, 78] and softwares [79]. We summarized in Table 2 the conditions that work for at least the cases studied in this work (that successfully generate current values or discharge morphologies agreeing well with the measurements).

The boundary conditions on cathodes when electron flows out are case dependent. In case of a pin–to–plane geometry or pin–to–pin geometry when finally the streamer will penetrate the gap and form a conductive channel, the electrons emitting from the cathode cannot be accurately predicted from a fixed secondary emission coefficient,

Table 2. Boundary conditions of continuity equations works for fast ionization waves, pin–to–plane discharges and nSDBD

Flux direction	Electron	Electron energy	Negative ion	Positive ion
Anode in	∇n=0	$\Gamma = \Gamma_e n_\epsilon$	∇n=0	0
Anode out	0	0	0	∇n=0
Cathode in	0	0	0	∇n=0
Cathode out	∇n=0 or $\Gamma = \gamma\Gamma_i$ (SDBD)	$\Gamma = \Gamma_e n_\epsilon$	∇n=0	0
Dielectric in	$\nabla \cdot \Gamma = 0$	$\Gamma = \Gamma_e n_\epsilon$	$\nabla \cdot \Gamma = 0$	$\nabla \cdot \Gamma = 0$
Dielectric out	$\Gamma = \gamma\Gamma_i$	$\Gamma = \Gamma_e \times 0.01$	0	0

thus a Neumann condition is set [80], otherwise the calculation crashes [41]. However for a surface dielectric barrier discharge, only by setting a secondary electron emission condition can we capture the cathode sheath region. The boundary conditions on dielectrics when charged particles flow in are checked. A first trial of ∇n=0 results in an overestimation of electrical current, while the $\nabla\Gamma$=0 boundary leads to more reasonable current values in comparison with experiments.

3.5. Gap closing strategies

As has been mentioned in the previous section, a conductive plasma channel forms when the streamer connects two metals. It is a common process in many applications, e.g. a spark plug [81].

Once the streamer approaches the ground, there will be a very high field between the ionization head and the cathode. Once the ionization head touches the end, a repulsion of the electric field leads to further increase of the electron density, and if the electric field in the channel is high enough to ionize the gas, the electron density will grow sharply and the non–equilibrium discharge may even transform into a thermal spark [9, 10].

The increased electron density reduces the dielectric relaxation time [16] below 10^{-5} ns or even lower, bringing larger computational cost. There exists three strategies treating the gap closing problem: (i) direct calculation regardless the computational cost [82]; (ii) "freeze" the electric field distribution and adjust the amplitude according to voltage changes; (iii) calculate electric field based on ambipolar approximation.

Strategy (ii) has been implemented in pin–to–pin discharge simulations [83, 84] and validated with measured currents [41]. This approach "freezes" the electric field distribution after the formation of conductive plasma channel and make the absolute value of electric filed changes proportionally to the applied voltage. This approach significantly accelerates the simulation with acceptable accuracy, but may fail in treating the pin–to–plane discharges when "side flares" or "branch streamers" appear at high voltages or very small curvature pin radius [41].

Strategy (iii) has been proved in calculation of gliding arc discharges [85–87] and

Table 3. Three strategies validated for calculating the closed discharge gap

Strategies	Timestep	Side streamers	Electron density
Direct calculation	$dt > 10^{-15}s$	✓	$n_e < 10^{22}$ m^{-3}
"Frozen field"	$dt < 10^{-15}s$	×	$n_e > 10^{22}$ m^{-3}
Ambipolar & Laplacian field	$dt < 10^{-15}s$	✓	$n_e > 10^{22}$ m^{-3}

streamer–to–spark transition [41]. The use of this approach is based on such a fact: the electron density gradient is much lower along the plasma conductive channel, and the timescale of chemical reactions significantly increases by about two orders of magnitude to $10^{-9} \sim 10^{-11}$ s compared with that of the discharge front in the streamer phase, this results in tiny charge separation and makes the ambipolar diffusion assumption reasonable.

We summary in Table 3 the three aforementioned strategies and corresponding application ranges. A simple selection criteria can be proposed here: if the average reduced electric field (defined by the voltage amplitude divided by the gap distance) is lower than the ionization threshold (e.g. 120 Td for air) in the conductive channel, it's possible that the time step $dt > 10^{-15}s$ and electron density $n_e < 10^{22}s$, direct calculation might work. Otherwise, strategy (ii) or (iii) have to be used. If there are side streamers produced due to very sharp pin curvature radius or ultrafast high voltage increase, only strategy (iii) can be used. In this work we use strategy (i) with the help of parallel acceleration.

4. Results and discussions

4.1. The discharge morphology

Calculations were conducted at atmospheric pressure and maximum voltages of 40, 68 and 86 kV for the diffusive ionization wave model and at moderate pressures (27 mbar and 40 mbar) with the voltage of 20kV amplitude for the fast ionization wave model.

The geometry of the volumetric diffusive ionization wave model are extracted from the experiments in Ref [38]: a metal conical pin (maximum diameter 1 mm, height 1 mm) connected with a metal cylinder and Trapezoidal revolution is the high voltage electrode; the pin and the ground are separated by a 16 mm gap. Figure 4 (a) shows the pin electrode shape and the mesh distributions (2 μm in size) near the tip. The voltage profiles with/out discharge are quite different, thus two voltage profiles are used for U_{max}=20 kV case and other cases, respectively, as is shown in Figure 4 (b).

The geometry and voltage profile of the fast ionization wave model can be found in our previous work [42] (with larger radius for the R=10 mm case), thus will not be replotted here.

The evolution of the discharge morphology (represented by electron density) and electric field distribution for the U_{max}= 86 kV case are shown in Figure 5 (a-f). The discharge is initiated near the pin tip, the high electric field leads to the formation

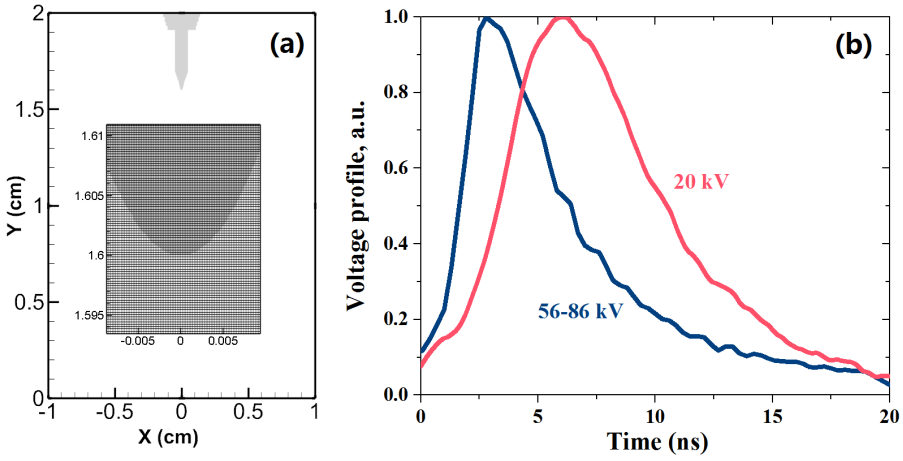

Figure 4. The geometry of the pin–to–plane configuration studied in Ref [38] (a) and the normalized voltage profiles applied on the pin electrode (b).

of a spherical discharge region at the beginning (Figure 5 (a) and (d)) due to field direct ionization [88]. The space charge and field distribution switches into a shell–shaped distribution due to charge separation (Figure 5 (b) and (e)), As the streamer approaches the ground, the ionization front is intensified and finally touches the end to form a conductive channel.

The transport dynamics of the diffusive ionization wave having similar sphere–to–shell transition have been analyzed in detail both experimentally [39, 88, 89] and numerically [21, 45]. Comparing with existing publications, two differences of discharge morphology are clearly seen. In this work: (i) there are always "side flares" or "side streamers" generated near the pin tip at the connection between conical pin and cylinder metal, however this phenomenon is not always seen in experiments. Only in a similar experiment reported in Ref [89] this "side flare" is observed. (ii) The maximum diameter (10 mm) of the diffusive streamer appears at z=9 mm position while in the experiments, the maximum diameter approaches 16 mm and the maximum appears at 13 mm.

Taking that the swarm parameters, the numerical schemes for transport and the kinetics scheme have been already validated by a series of previous works, the first trial looking for the reasons of the differences is to change the pin shape. We found that varying merely the curvature radius of the pin tip from 50∼100 μm has negligible influence on the discharge evolution, but the overall shape of the conical pin affects significantly the calculated discharge morphology.

Three pins with distinct shapes are tested for the U_{max}= 86 kV case: an elliptical, a triangle and the experimentally defined shape. Using exactly the same voltage profile, swarm parameters, kinetics and numerical schemes, we see significant differences in the formation of the "side flares" and the diffusive streamer morphology, see Figure 6 (a)–(c).

The length and the direction of the "side flares" are related with the sharpness, smoothness and z–direction slope of the pin shape. In Figure 6 (a) the elliptical pin

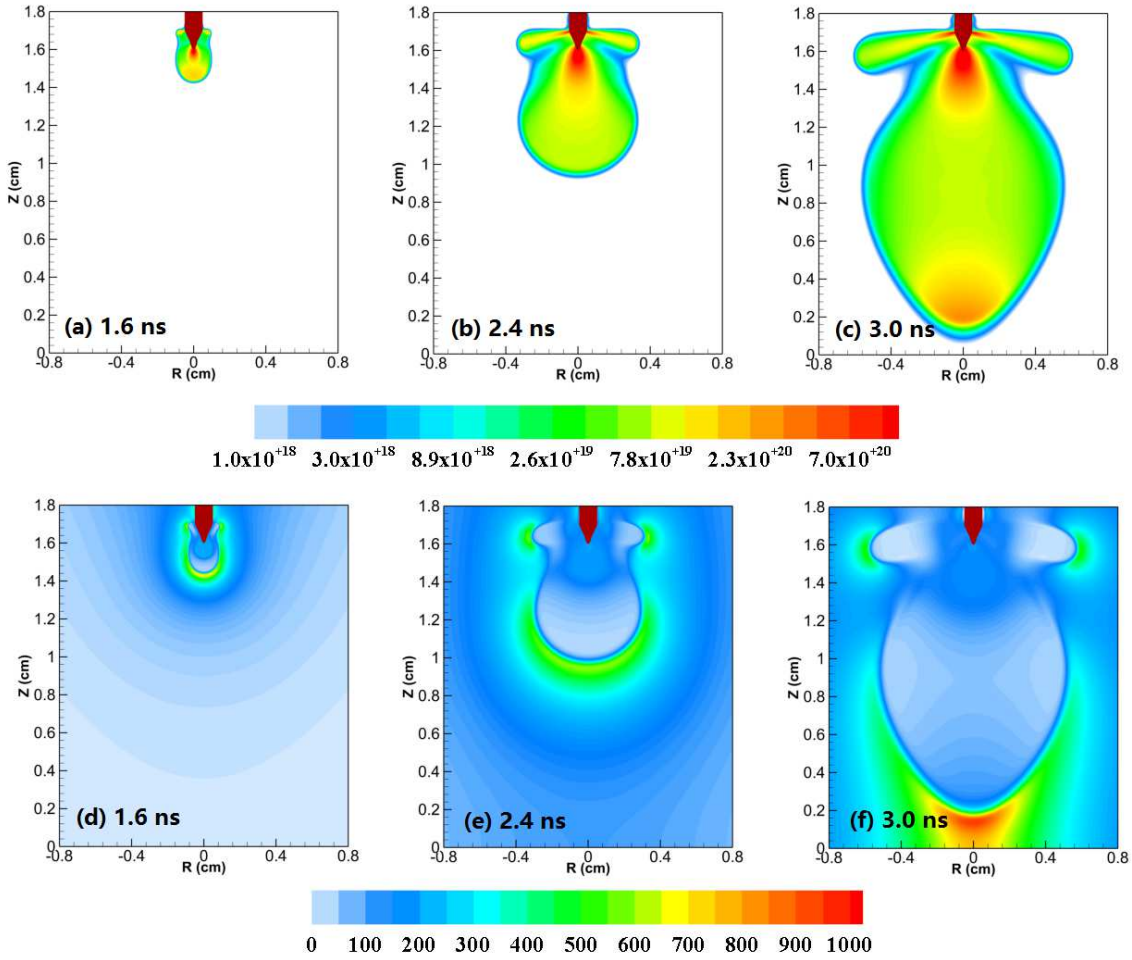

Figure 5. The evolution of the diffusive volumetric ionization wave during the propagation stage (unit in m^{-3}). (a–c) The electron density and (d–f) the reduced electric field (unit in Td).

shape ensures the smoothness of the pin, the starting point of the main streamer and the side streamers almost merge, the calculated diameter agrees well with the measurement, the maximum diameter position is elevated to 12.2 mm. In case of the triangle shape, the main streamer is initiated on the very sharp pin tip, while the side streamers appear on the upper side, the diameter of the main diffusive ionization wave is not affected but the maximum position drops to z=104 mm, see Figure 6 (b). For the experimentally defined pin shape, the very sharp corner above the pin tip results in quite strong side streamers propagating perpendicular to the shape surface, the high electric field induced by the side streamers (∼500 Td, comparable with the main streamer) strongly affects the morphology of the main diffusive ionization waves.

Experimentally, the "side streamers" are not always seen near the pin tip, but the fluid model with exactly the same geometry will always lead to the same results. We have conducted a careful check to exclude the possibilities from boundary conditions. Further studies (will see in Figure 10) shows that, if the curvature radius of the pin

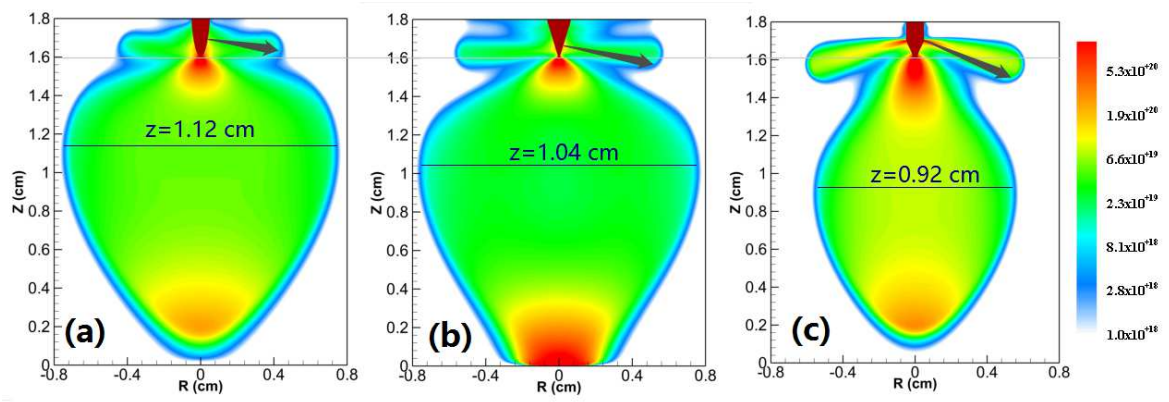

Figure 6. The discharge morphology at the moment of penetration driven by the same applied voltage (86 kV) triggered form the pin electrodes with different shapes. The pin shapes are defined by (a) an ellipse, (b) a triangle and (c) the close–to–experiment measurement.

is small enough, and if there are pre–distributed electrons nearby, there will always be streamers formation from the tip and the sharp corners. In the simulation of this work, we always have at least 1 electrons per cubic meter (to prevent numerically the possible "divided by 0" problem), thus we will always have side streamers in the simulation. In a trial experiment, we have found that, if an nanosecond pulse is applied to the pin right after a negative DC voltage, the side streamers can be reproduced repeatedly, while if we directly apply the nanosecond voltage pulse, there will be only one diffuse streamer: this phenomenon indicates that, the presence of seed electrons near the pin might be the key to the appearance of "side streamers".

One of the solutions to suppress the "side streamers" numerically, is to artificially adjust the pin shape (but keeping a fixed curvature radius), thus one can simulate the discharge streamer morphology agreeing well with the observations. The use of this strategy can be found in Ref [21, 45]. Another solution is to exclude the pin shape from the computational domain, thus the streamer will be initiated only from a point (the pin tip).

In this work, we still use the experimentally defined shape in the following analysis to ensure a direct comparison. The electric field in experiments is measured near the pin tip, which can be sensitive to the pin shape. A test calculation of the axial Laplacian field at the probing point (3 mm away from the tip) with different pin shapes have been conducted and plotted together with E–FISH measured data and reference calculation [38] in Figure 7 (a), the geometry used in this work gives the most accurate results. We also tracked the time dependent ionization front position (defined by the $N_2(C^3\Pi_u)$ density) and plot the z–t diagram together with the measurements (conducted in a 18 mm gap with maximum voltages U_{max}=86, 75 and 65 kV) in Figure 7 (b), a good agreement is achieved, indicating that the diffusive streamer propagation velocity is not strongly affected by the side streamers or pin shapes.

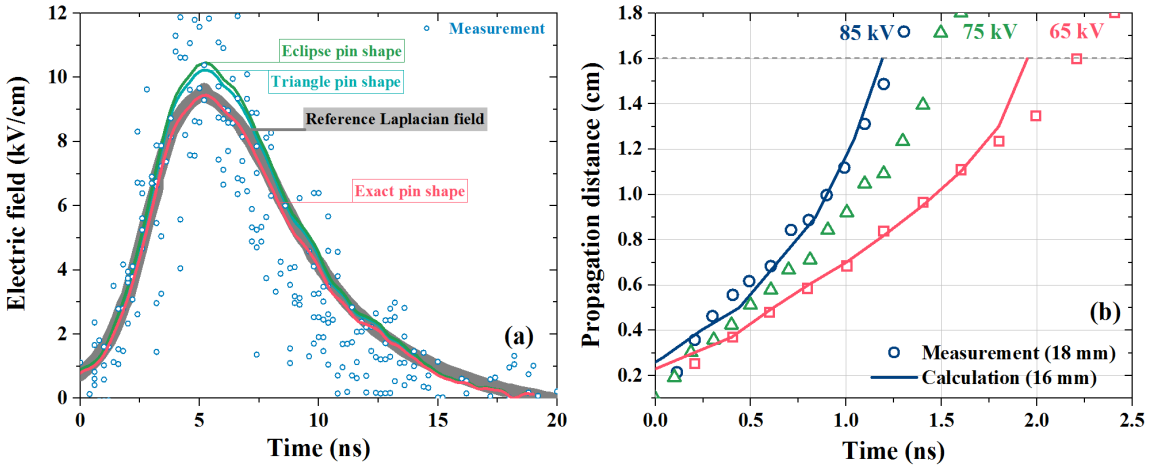

Figure 7. Test calculations of electric fields with different pin shapes and the streamer propagation. (a) The axial Laplacian field calculated with Eclipse, triangle and measured pin shape for U_{max}=20kV case. The experimental circles are extracted from Ref [38]. (b) The z-t diagram of streamer front calculated in 16 mm gap and measured in 18 mm gap at different voltage profiles, the measured values in scatters are extracted from Ref [90].

4.2. The field evolution at the probing point

A direct comparison of the measured and calculated absolute electric fields (axial fields) of the diffusive ionization wave and the fast ionization wave at fixed probing points is shown in Figure 8 (a)–(d). We note that in experiments, the E–FISH signal is collected as a line integral of intensity, thus the first question before systematic comparisons is, what data from numerical simulation should we use? It can be a line integral of the absolute electric field along the laser trace, or an integral multiplied with a Voigt function representing the distribution of the laser intensity, or just the point axial electric field. We conducted a trial calculation for the volumetric diffusive ionization wave and found that the time evolutions of the electric fields obtained by the first 2 options are totally different from the measurements, on the contrary, the calculated point axial field gives reasonable results, thus all the discussions below are conducted based on the calculated axial fields at the fixed point. The situation of the fast ionization wave (R=10 mm case) is more complicated, as the discharge in a low pressure tube exhibits a "hollow" discharge structure, the ionization wave propagates along the tube boundary, the highest electric field appears not in the tube center but near the surface, the near surface electric field could be several times higher than the axis field. In this work we only probe the calculated axis field for a comparison.

The probed point field evolutions can be divided into three categories.

(i) The ionization wave does not touch the end. This is the case of U_{max}=40 kV shown in Figure 8 (a). The axial field grows until the ionization front passed, followed by a sharp drop of the field. then the field decreases slowly following the voltage profile till 0.

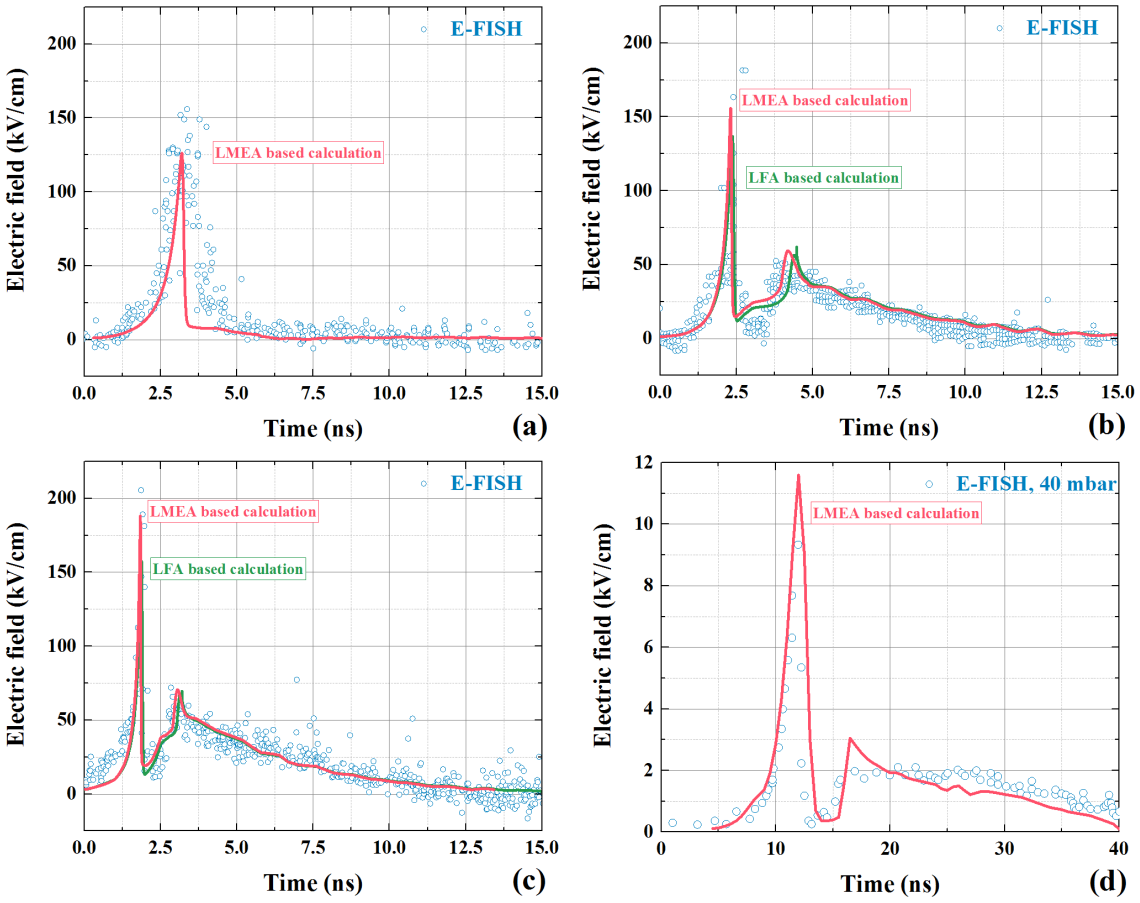

Figure 8. Comparison between calculated axial electrical field and E–FISH measurements of the atmospheric diffusive ionization wave and moderate pressure fast ionization wave discharges. (a) U_{max}=40 kV case, (b) U_{max}=68 kV case and (c) U_{max}=86 kV case in the diffusive ionization wave, (d) the field of the fast ionization wave case. The red lines are calculated fields based on LMEA and green based on LFA, the circles are measured E–FISH results extracted from Ref [37, 38]. The fields in (a–c) are extracted 3 mm away from the pin, the field in (d) is probed at the center of the tube.

(ii) The ionization wave penetrates the gap and a conductive channel forms, as shown in Figure 8 (b) and (c). The increase of voltage amplitude reduced the time gap between the first and the second field peak. A sharp jump in the rising period of the second peak is observed both in measurements and simulations (note that a simple average of the points may miss this physics). After the channel is closed, the field just decrease according to the voltage profiles. The peak field is 170 and 200 kV/cm in experiments but 150 and 180 kV/cm in simulation, a 20 kV/cm gap in field always exists. In the recent simulation work of the diffusive streamer [45], a peak field above 200 kV/cm is achieved numerically with time sampling of 0.01 ns. The working condition in Ref [45] is 55 kV peak voltage and 16 mm gap distance, similar to the case in this work, but the voltage rising time in Ref [45] is 0.5 ns, much shorter than the 2.5 ns experimental condition, the pin is 100 μm in radius, much smaller than the

cylindrical metal radius 1 mm. Both the pin sharpness and the voltage rising time affect significantly the inception of the discharge (the influence of voltage rising time will be discussed in section 4.3), the thinner pin leads to increased field as shown in Figure 7 (a), and the shorter rising voltage leads to higher electric field and energy deposition in the voltage rising slope, this is also confirmed in a recent calculation of nSDBD with voltage rising time ranging from 10 ps to 400 ns [91].

(iii) The ionization wave passes through the probe point and propagates a long distance (40 mm) to close the gap, see Figure 8 (d). This is the case of fast ionization wave propagating in the long tube. We do not find the E–FISH results under 27 mbar thus the measured results at 40 mbar are plotted together with the calculated values. The calculated axial field agrees with the measurement in the field rising slope, the calculated peak value (11–12 kV/cm) is slightly higher than the measured one (10 kV/cm, corresponding to 1000 Td). If we reduce the tube radius from 10 mm to 0.75 mm, the electric field in the ionization head would increase dramatically to 10000 Td, exceeding the application range of the fluid model, but not affect the kinetics processes in the plasma channel [42]. If one requires more accurate modeling of (the developing stage of) capillary discharges using a fluid model, increasing the radius or ambient pressures would be preferable. After gap closing, field across the quasi–uniform plasma region follows the variation of the voltage pulse.

We have conducted test calculations based on both LMEA and LFA for the diffusive ionization wave case, Figure 8 (b) and (c) shows clearly that for a volumetric streamer, the two approximations lead to similar results, agreeing well with the measurements. However at the moment of inception and gap closing, some details are not clearly specified: the "shoulder" at the inception stage and the field repulsion at the gap closing stage, which will be discussed in detail in the following section.

4.3. The inception of the streamer

The concrete sources of seed electrons initiating the first inception are still subjects for discussion. There is scant information on the very first inception development that compares directly with the experiments. A common approach in numerical simulation is to predefine a distribution of low density seed electrons (and ions) in the computational region, and use photo–ionization to sustain the positive streamer propagation. However this approach may lead to a "fake" discharge or miss the "shoulder" phenomenon:

(1) The "fake" discharge inception in the simulation

In section 4.1 we have compared the calculated Laplacian field of U_{max}= 20 kV case and achieved a good agreement with the reference, see Figure 7 (a). Ideally even if we solve all plasma equations, there should be no streamer formation like what we will see in experiments of Ref [38]. However, what we see is the green curve marked "Plasma on" in Figure 9 (a). The increase of electric field indicates that the fluid model predicts a "fake" streamer.

We first checked whether or not a streamer could form at this condition by probing

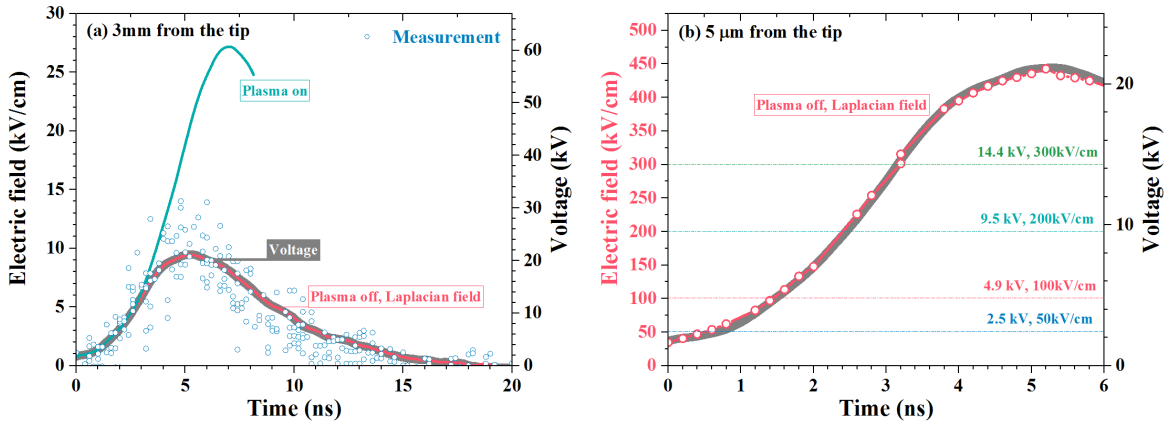

Figure 9. The field–voltage profiles near the pin electrode. (a) The comparison between calculated electric field (blue line), the Laplacian field (red line) and voltage profile (grey line). The experimental values in blue scatters are extracted from Ref [38]. (b) The Laplacian field and voltage profile 3 mm and 5 μm away from the pin tip.

numerically the Laplacian field 5 μm (2-3 mesh grids size) down the pin tip, shown in Figure 9 (b). The field reaches as high as 450 kV/cm, 14 times larger than the ionization threshold field of air (32 kV/cm), the electric field is high enough to initiate a streamer discharge. To further check the time cost of streamer initiation, we selected 4 typical moments in Figure 9 (b) (the cross point of the dash dot lines and the field curve) and calculated the streamer formation time for a constant electric field based on the classical Raether-Meek criterion, the formula writes [92]:

$$\tau_{\text{streamer}} = \ln(\mathrm{g}(E) \cdot N_0/N)/(\alpha_{\mathrm{T}}\mu_e E) \tag{19}$$

where $\mathrm{g}(E) \approx 10^8$ is a commonly used empirical approximation, $N_0 = 2.45 \times 10^{25}$ m^{-3} is the gas density at standard temperature and pressure, $N = N_0$ is the gas density at studied condition, α_{T} and μ_e are the effective Townsend ionization coefficient and mobility of electrons, respectively, E is the electric field. The meaning of equation (19) is the time used to form the electron density of $\mathrm{g}(E) \cdot N_0/N$, the value is the required electron density for streamer formation.

The calculated streamer formation time τ_{streamer} is drawn in Figure 10 (a). At the time instant of 3–4 ns, the streamer would form within 0.04 ns according to equation (19). We also plotted the calculated evolution of electric field near the pin tip in the beginning 4 ns (Figure 10 (b)), the ionization front forms and develops after 3 ns.

We also tried to reduce the seed electron density to an extremely low value (10 m^{-3} evenly distributed in the entire domain), however we still see the formation and propagation of the streamer due to the presence of photo–ionization and strong electric field. If we estimate the growth of the electron density simply according to $n_e(t) = n_e(t = 0)exp(\alpha_{\mathrm{T}}\mu_e E)$, we will have an electron density of 10^{17} m^{-3} within 0.1 ns at 300 kV/cm. Thus, there should be no free electrons near the pin tip in the

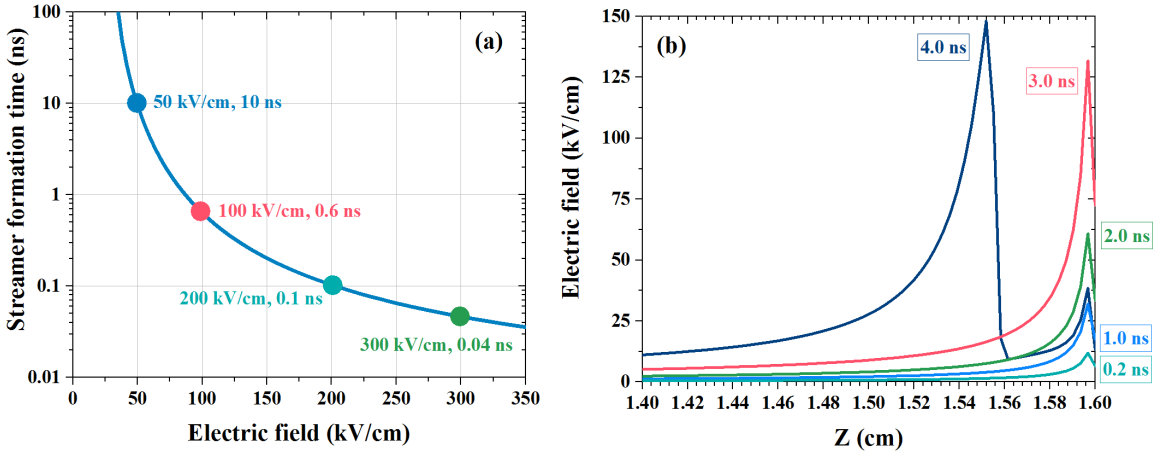

Figure 10. The streamer formation time and axial field distribution. (a) The theoretical streamer formation time calculated for different constant electric field, the marked points correspond to the sample lines marked in Figure 7 (b). (b) The calculated axial electric field for U_{max}= 86 kV case.

experiments, and this cannot be represented by the predefined average electron density in the space.

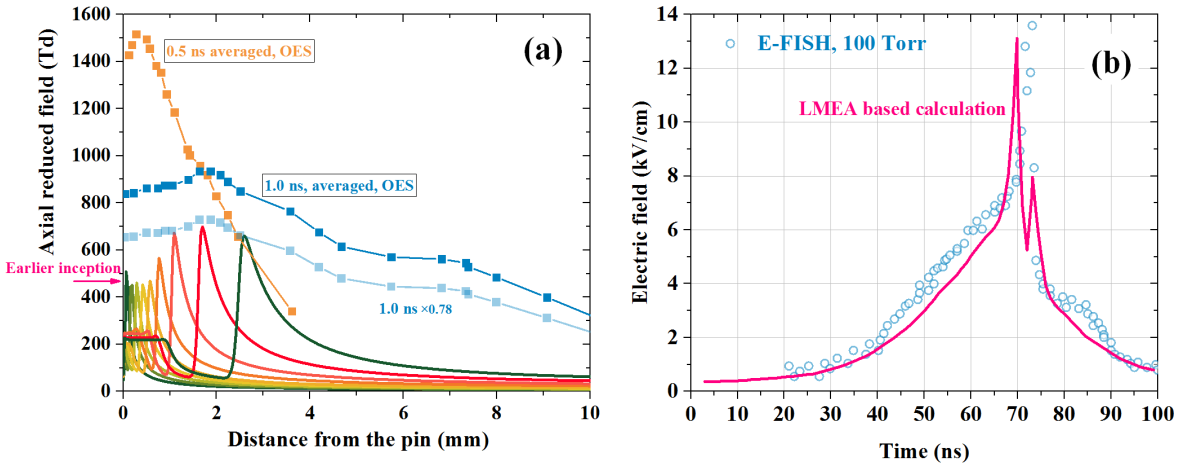

Figure 11. The influence of seed electrons. (a) The pin–to–plane discharge in air: comparison between the temporal and spatial averaged electric field measured by OES [93] and the calculated electric field within 10 mm from the pin. (b) The DBD discharge in N_2: comparison between the E–FISH measured field [31] and the calculated electric field (with a high seed electron density of $n_e = 6 \times 10^{15}\ m^{-3}$).

The influence of the seed electrons can be further confirmed by comparing calculation with the optical emission spectrometry experiment of the diffusive streamer discharge [93], and with the E–FISH measurement of a pre–ionized dielectric barrier discharge [31] in Figure 11.

The spatial and temporal averaged distribution of electric field measured by OES (line with symbols) at 0.5 ns and 1.0 ns is plotted together with the calculated time

resolved electric field in Figure 11 (a). At the inception stage, the measured electric field is significantly higher than the prediction (with seed electrons of $10^9 cm^{-3}$), indicating that the inception voltage in the experiment is much higher than in the simulation. The delay of the inception in the experiment leads to higher field near the pin, the calculated field is about 0.78 times smaller than the measurement, as has also been shown in Figure 8. In Figure 11 (b), The E–FISH measured time resolved electric field of a pre–ionized dielectric barrier discharge in pure nitrogen is plotted together with the calculation. In both the experiment and simulation, there are enough seed electrons, thus the discharge inception is not delayed and the peak field agrees well with each other.

To simulate correctly the inception moment in case of extremely fast voltage pulse with no seed electrons, one may has to either introduce some stochastic processes (i.e. to predefine a situation when there is no free electrons at all near the pin tip) or introduce some new physics (i.e. considering the flux emission from cathodes due to secondary electron emission and instant detachment from the desorbed negative ions [94]).

(2) The discharge "shoulder" in the measurements

The measured points exhibit a "shoulder" stage between 0 to 2 ns when the electric field is higher than the predicted field (or the Laplacian field), see Figure 12 (a). A similar "shoulder" can be found in the inception stage (0–10 ns) of the fast ionization wave discharge in a capillary tube (R=0.75 mm) at 27 mbar, as shown in the green line of Figure 12 (b), although the field detected by the capacitive probe is measured outside the tube, we still do not get numerically the "shoulder" region in the first 10 ns at the same probing position. But it is interesting that the E–FISH measurement of the fast ionization wave discharge do not have the shoulder.

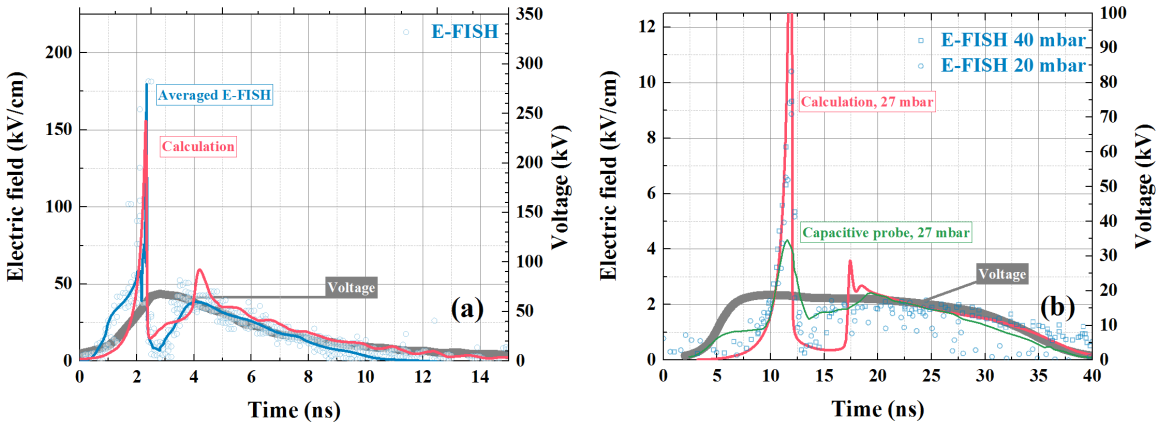

Figure 12. The "shoulder" problems. (a) The comparison between calculated (red lines) and measured (blue lines for average and blue circles for exact values [38]) axial electric field 3 mm away from the pin tip in the diffusive ionization wave condition. (b) The comparison between calculated (red lines) axial electric field and measured (green lines from capacitive probe measurements [36]) out of the capillary tube (R=0.75 mm) in the fast ionization wave discharge, E–FISH data (R=10 mm) [37] in circles and squares are plotted for reference.

The mechanism for this "shoulder" discharge is still unknown. This phenomenon gives an impression that a weak ionization wave forms prior to the main ionization wave, additional physical model has to be introduced to reproduce accurately such phenomenon. Ref [95, 96] used a priori a small-sized cloud of seed electrons pre–existing at the cathode and distributed according to a Gauss curve (in both radial and longitudinal direction) to simulate the development of an isolated transverse-inhomogeneous microdischarge. By locally distributing electrons near the cathode, it is possible to raise the electric field higher than the Laplacian field before the clouds touches the anode and starts the discharge. We have made a trial calculation with this approach by setting seed electrons only at the cathode (10^{10} m^{-3}), however, the "shoulder" is still not seen.

The combination of the "fake" inception and "shoulder" discharge problems make it a challenge to accurately simulate the inception of the streamer discharge initiated by extremely fast rising voltage (below 2.5 ns in this work). A compromise way would be reducing artificially the voltage rising time to a very small value to skip this stage and focus only on the development stage of the streamer discharge, other strategies includes introducing stochastic processes or employ new physics on the cathode boundaries taking that the processes of desorption of ions from cathode and electrons from negative ions.

4.4. The evolution of the conductive channel

A comparison of the discharge morphologies between the simulation and the experiment [90] after gap closing is presented in Figure 13. (a)–(f) is the distribution of calculated $N_2(C^3\Pi_u)$ while (a')–(f') is the experimentally observed emission intensity.

The discharge are driven by the same pin shape and voltage profile but the gap in the experiment is 18 mm. The color map in the experimental figures is not uniform thus the comparison shown in Figure 13 is rather qualitative. Once the ionization head touches the end, the discharge shrink from the conical structure to a column, with intensive emission near the pin and ground. With the decrease of the applied voltage, the emission decays firstly in the central channel, finally only the glow on the pin tip can be observed both in calculation and in experiment.

The nanosecond pulsed diffusive discharge is promising in gas de–pollution or transformation, the gap closing stage is of great importance as the energy deposition and gas heating happened mainly in this stage. The electric field evolution at the junction moment affects the initial value of species density that can be used in a simple global model. The field evolutions before and after the junction for the U_{max}= 86 kV and U_{max}= 68 kV case are plotted in Figure 14 (a) and (b).

Figure 14 shows an increase of the field value above the average gap field defined by U/d due to the repulsion of the electric field. This explains for the sharp jump up and down of electric field in the second electric field peak in Figure 8. After the jump, the field decays and the evolution can be described directly by the Laplacian field, making it possible for further global kinetics analysis(e.g. Ref [41]) and development of

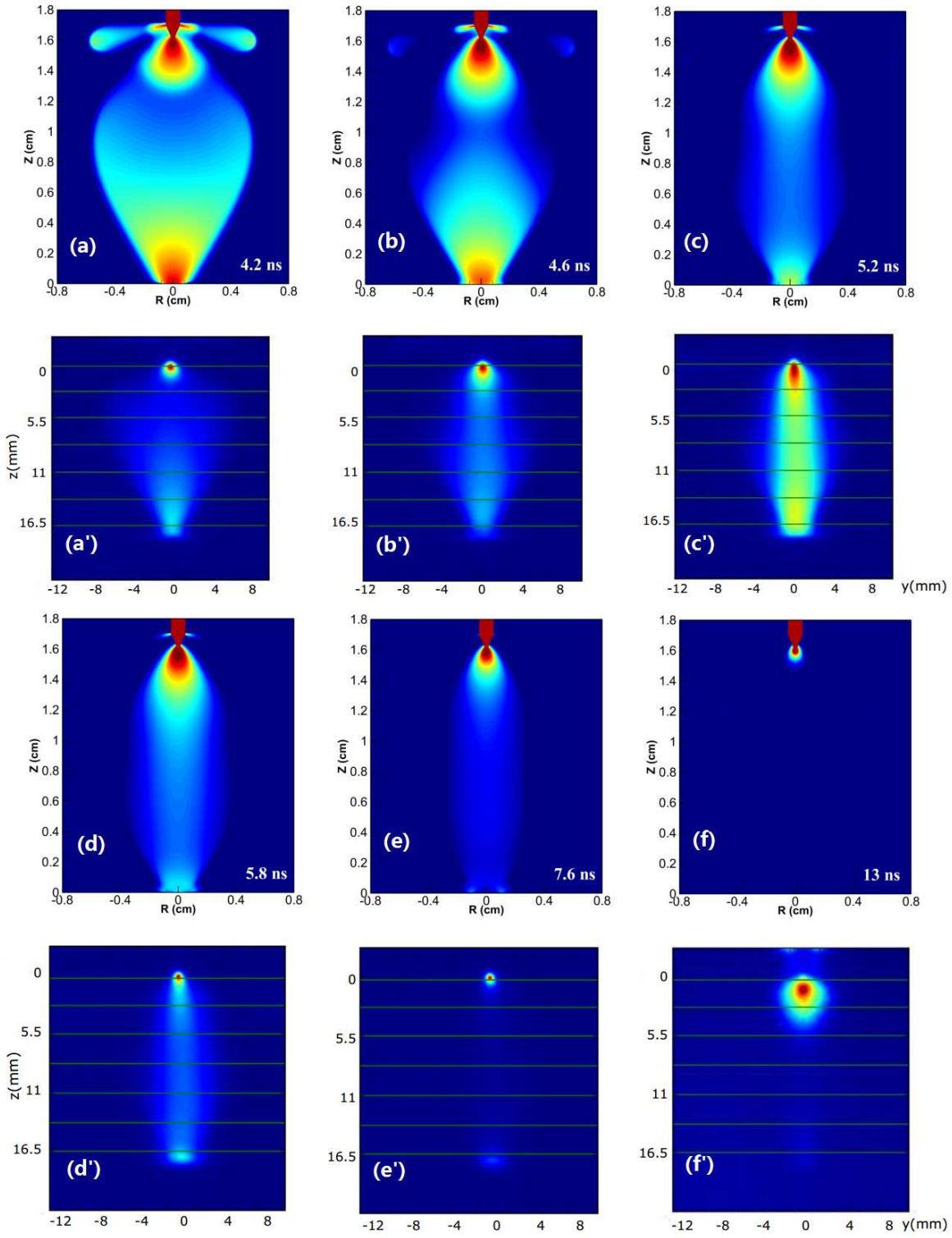

Figure 13. A qualitatively comparison of spatial–temporal evolution of discharge morphology after gap closing between simulation and experimental observation for the U_{max}= 86 kV case. (a)–(f) the calculated $N_2(C^3\Pi_u)$ distribution in the 16 mm gap, (a')–(f') the emission intensity distribution in the 18 mm gap. The time moment and color scale are not exactly the same between the simulation and experiment. The experimental photos are taken from Ref [90].

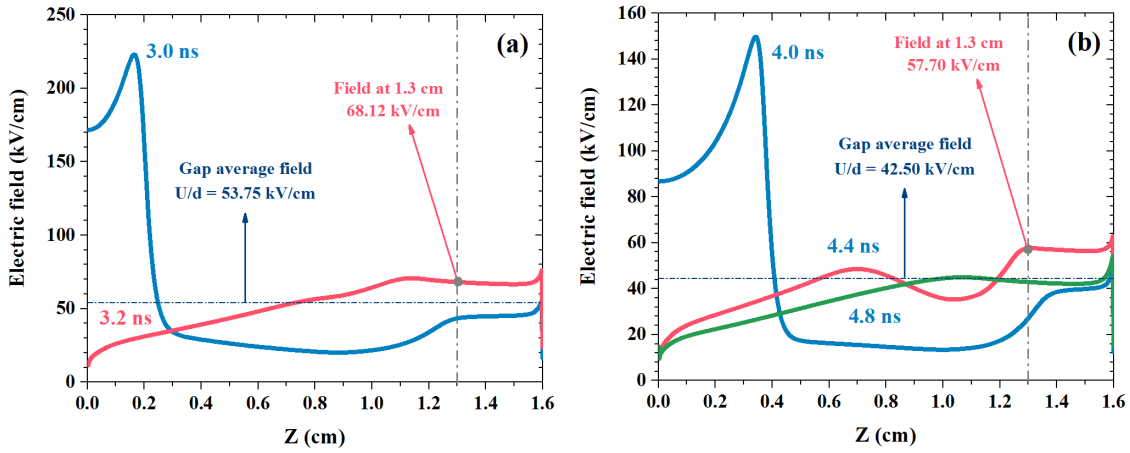

Figure 14. The evolution of the axial electric field right before and after the streamer touching the ground for the (a) U_{max}= 86 kV and (b) U_{max}= 68 kV case.

programmable plasma chemistry pathway.

5. Conclusions

In this work, direct comparisons between fluid modeling and recent measurements of a diffusive ionization wave driven by extremely fast voltage pulse and fast ionization wave having very high electric field are conducted. The numerical simulations are conducted using on a validated code, *PASSKEy*.

A pressure–E/N application range of the drift–diffusion approximation is defined taking that the inertial term has much smaller influence than collisions term and the momentum transfer characteristic time scale is much shorter than the case time scale. The region satisfying E/N<2000 Td and pressure>0.5 mbar is the sweet region for the drift–diffusion fluid plasma model (Figure 1).

A pressure–grid range of the local field/mean energy approximation is proposed for discharges containing interaction with dielectric surfaces. If the mesh grids used in the simulation is smaller than the critical sheath size $T_{es}n_{emax}/E_s/n_{eavg}$, the local mean energy approximation is preferred, otherwise both approximations give similar results, e.g. volumetric streamers (Figure 2).

The three–terms Helmholtz photo–ionization is extended into a more general form with recommended fitting parameters for N_2, O_2, CO_2 and air are provided with corresponding *pr* range. This extended Photo–ionization model makes it possible to calculate photo–ionization sources for streamer discharges in any gases with calculated or measured photo–ionization functions.

The calculated discharge morphology is affected by the pin shape due to the presence of "side flares" (which is not always seen in the experiments due to stochastic process and lack of seed electrons) initiated near the sharp corners of the pin electrodes. The appearance of the "side flares" does not affect the field near the pin and the

propagation velocity of the main streamer. By reducing the pin electrode into a combination of very thin cylinder with a round tip, the "side flares" can be suppressed and a more close–to–observation morphology can be achieved, but the predicted field near the pin tip will be higher than in measurements.

The calculated electric field evolutions in the diffusive ionization wave and the fast ionization wave in a bounded tube are compared with E–FISH measurements at probing points, to authors' knowledge, it is the first direct comparison between E–FISH measurements and two dimensional numerical simulation at the same geometry and working conditions. A good agreement in electric field profile is achieved, the predicted peak field is always 20 kV/cm lower than the measurement in the atmospheric diffusive ionization wave, while 1-2 kV/cm higher than the fast ionization wave case at moderate pressure (40 mbar). By reducing the tube radius (from 10 mm to 0.75 mm) the field in the head of the fast ionization wave increases to an extremely high value (>10000 Td). The difference in peak field value indicates that, we must remain critical about the field strength derived from the E–FISH technique as detailed in Ref [38], On the other side, even if there are some issues still to be addressed with E–FISH, experimental measurements remains coherent with simulation and with previous results obtained by OES [93].

Before the discharge inception, a predefined electron density averaged in the entire computational domain may either predict a "fake" streamer when the discharge is not initiated, or predict an electric field lower than the measured "shoulder". The first phenomenon may be solved by artificially introducing some stochastic processes (e.g. predefine some conditions when there are no electrons at all near the pin tip) or additional physical processes (i.e. considering the flux emission from cathodes due to secondary electron emission and instant detachment from the desorbed negative ions), but the reason for the second discrepancy ("shoulder") is not clear yet. It is recommended that one may skip the inception stage when conducting fluid modeling and focus more on the streamer development and conduction stage, in which much higher accuracy can be achieved.

The conductive channel is also modeled. At the moment streamer touching the ground, the field repulse leads to a jump of the electric field in the channel, the field is higher than the average electric field defined by U/d. The transition from the conical structure to a conductive column is observed in both simulation and experiments.

Acknowledgements

The work is supported by the National Natural Science Foundation of China No. 51907204, 51790511, 91941105, 91941301 and 52025064. The authors are thankful to Prof. Svetlana Starikovskaia, Prof. Igor Adamovich and Dr. TatLoon Chng for half year's fruitful discussions concerning experimental measurements, and to Prof. G V Naidis for helpful advices on the fluid model. We are also thankful to the young research group in Atelier des Plasmas (Gongfang) for maintenance of the *PASSKEy* code.

References

[1] B. Eliasson and U. Kogelschatz, "Nonequilibrium volume plasma chemical processing," *IEEE transactions on plasma science*, vol. 19, no. 6, pp. 1063–1077, 1991.

[2] H. Biederman, *Plasma polymer films*. World Scientific, 2004.

[3] V. E. Gusev and A. A. Karabutov, "Laser optoacoustics," *NASA STI/Recon Technical Report A*, vol. 93, 1991.

[4] H.-H. Kim, "Nonthermal plasma processing for air-pollution control: a historical review, current issues, and future prospects," *Plasma Processes and Polymers*, vol. 1, no. 2, pp. 91–110, 2004.

[5] Y. Ju and W. Sun, "Plasma assisted combustion: dynamics and chemistry," *Progress in Energy and Combustion Science*, vol. 48, pp. 21–83, 2015.

[6] A. Fridman, A. Chirokov, and A. Gutsol, "Non-thermal atmospheric pressure discharges," *Journal of Physics D: Applied Physics*, vol. 38, no. 2, p. R1, 2005.

[7] A. Y. Starikovskii, A. Nikipelov, M. Nudnova, and D. Roupassov, "SDBD plasma actuator with nanosecond pulse-periodic discharge," *Plasma Sources Science and Technology*, vol. 18, no. 3, p. 034015, 2009.

[8] F. Massines, P. Segur, N. Gherardi, C. Khamphan, and A. Ricard, "Physics and chemistry in a glow dielectric barrier discharge at atmospheric pressure: diagnostics and modelling," *Surface and Coatings Technology*, vol. 174, pp. 8–14, 2003.

[9] N. Minesi, S. Stepanyan, P. Mariotto, G. D. Stancu, and C. O. Laux, "Fully ionized nanosecond discharges in air: the thermal spark," *Plasma Sources Science and Technology*, vol. 29, p. 085003, aug 2020.

[10] N. Q. Minesi, P. B. Mariotto, G.-D. Stancu, and C. O. Laux, "Ionization Mechanism in a Thermal Spark Discharge," in *AIAA Scitech 2021 Forum*, no. January, (Reston, Virginia), pp. 1–19, American Institute of Aeronautics and Astronautics, jan 2021.

[11] J. Teunissen, "Improvements for drift-diffusion plasma fluid models with explicit time integration," *Plasma Sources Science and Technology*, vol. 29, no. 1, p. 015010, 2020.

[12] J.-P. Boeuf and L. C. Pitchford, "Pseudospark discharges via computer simulation," *IEEE Transactions on Plasma Science*, vol. 19, no. 2, pp. 286–296, 1991.

[13] S. Rauf and M. J. Kushner, "Dynamics of a coplanar-electrode plasma display panel cell. i. basic operation," *Journal of applied physics*, vol. 85, no. 7, pp. 3460–3469, 1999.

[14] P. Viegas, F. Pechereau, and A. Bourdon, "Numerical study on the time evolutions of the electric field in helium plasma jets with positive and negative polarities," *Plasma Sources Sci. Technol.*, vol. 27, no. 2, p. 025007, 2018.

[15] A. Dubinova, D. Trienekens, U. Ebert, S. Nijdam, and T. Christen, "Pulsed positive discharges in air at moderate pressures near a dielectric rod," *Plasma Sources Science and Technology*, vol. 25, no. 5, p. 055021, 2016.

[16] P. Vitello, B. Penetrante, and J. Bardsley, "Simulation of negative-streamer dynamics in nitrogen," *Physical Review E*, vol. 49, no. 6, p. 5574, 1994.

[17] G. Naidis, "Modelling of streamer propagation in atmospheric-pressure helium plasma jets," *Journal of Physics D: Applied Physics*, vol. 43, no. 40, p. 402001, 2010.

[18] A. M. Lietz, E. Johnsen, and M. J. Kushner, "Plasma-induced flow instabilities in atmospheric pressure plasma jets," *Applied Physics Letters*, vol. 111, no. 11, p. 114101, 2017.

[19] N. Y. Babaeva, D. V. Tereshonok, and G. V. Naidis, "Fluid and hybrid modeling of nanosecond surface discharges: effect of polarity and secondary electrons emission," *Plasma Sources Science and Technology*, vol. 25, no. 4, p. 044008, 2016.

[20] Y. Zhu, S. Shcherbanev, B. Baron, and S. Starikovskaia, "Nanosecond surface dielectric barrier discharge in atmospheric pressure air: I. measurements and 2D modeling of morphology, propagation and hydrodynamic perturbations," *Plasma Sources Science and Technology*, vol. 26, no. 12, p. 125004, 2017.

[21] F. Pechereau, P. Le Delliou, J. Jánskỳ, P. Tardiveau, S. Pasquiers, and A. Bourdon, "Large conical

discharge structure of an air discharge at atmospheric pressure in a point-to-plane geometry," *IEEE Transactions on Plasma Science*, vol. 42, no. 10, pp. 2346–2347, 2014.

[22] Y. Zhu, Y. Wu, B. Wei, H. Liang, M. Jia, H. Song, X. Haojun, and Y. Li, "nSDBD based plasma assisted anti-icing: modeling and mechanism analysis," *Journal of Physics D: Applied Physics*, vol. 53, p. 145205, 2019.

[23] B. Bagheri, J. Teunissen, U. Ebert, M. M. Becker, S. Chen, O. Ducasse, O. Eichwald, D. Loffhagen, A. Luque, D. Mihailova, J. M. Plewa, J. van Dijk, and M. Yousfi, "Comparison of six simulation codes for positive streamers in air," *Plasma Sources Science and Technology*, vol. 27, p. 095002, sep 2018.

[24] B. M. Goldberg, I. Shkurenkov, S. O'Byrne, I. V. Adamovich, and W. R. Lempert, "Electric field measurements in a dielectric barrier nanosecond pulse discharge with sub-nanosecond time resolution," *Plasma Sources Science and Technology*, vol. 24, p. 035010, may 2015.

[25] P. B?Hm, M. Kettlitz, R. Brandenburg, H. H?Ft, and U. Czarnetzki, "Determination of the electric field strength of filamentary dbds by cars-based four-wave mixing," *Plasma Sources Science Technology*, vol. 25, no. 5, p. 054002, 2016.

[26] A. Dogariu, B. M. Goldberg, S. O. Byrne, and R. B. Miles, "Species-Independent Femtosecond Localized Electric Field Measurement," *Physical Review Applied*, vol. 7, p. 024024, 2017.

[27] B. M. Goldberg, L. Chng, A. Dogariu, and R. B. Miles, "Electric field measurements in a near atmospheric pressure nanosecond pulse discharge with picosecond electric field induced second harmonic generation," *Applied Physics Letters*, vol. 112, p. 064102, 2018.

[28] I. V. Adamovich, T. Butterworth, T. Orriere, D. Z. Pai, D. A. Lacoste, and M. S. Cha, "Nanosecond second harmonic generation for electric field measurements with temporal resolution shorter than laser pulse duration," *Journal of Physics D: Applied Physics*, vol. 53, no. 14, p. 145201, 2020.

[29] M. S. Simeni, B. M. Goldberg, C. Zhang, K. Frederickson, W. R. Lempert, and I. V. Adamovich, "Electric field measurements in a nanosecond pulse discharge in atmospheric air," *Journal of Physics D: Applied Physics*, vol. 50, no. 18, p. 184002, 2017.

[30] B. Huang, C. Zhang, I. Adamovich, Y. Akishev, and T. Shao, "Surface ionization wave propagation in the nanosecond pulsed surface dielectric barrier discharge: the influence of dielectric material and pulse repetition rate," *Plasma Sources Science and Technology*, vol. 29, p. 044001, mar 2020.

[31] K. Orr, X. Yang, I. Gulko, and I. V. Adamovich, "Formation and propagation of ionization waves during ns pulse breakdown in plane-to-plane geometry," *Plasma Sources Science and Technology*, vol. 29, p. 125022, dec 2020.

[32] K. Orr, Y. Tang, M. Simeni Simeni, D. van den Bekerom, and I. V. Adamovich, "Measurements of electric field in an atmospheric pressure helium plasma jet by the E-FISH method," *Plasma Sources Science and Technology*, vol. 29, p. 035019, mar 2020.

[33] T. L. Chng, S. M. Starikovskaia, and M.-C. Schanne-Klein, "Electric field measurements in plasmas: how focusing strongly distorts the E-FISH signal," *Plasma Sources Science and Technology*, vol. 29, p. 125002, dec 2020.

[34] N. D. Lepikhin, D. Luggenhölscher, and U. Czarnetzki, "Electric field measurements in a He:N 2 nanosecond pulsed discharge with sub-ns time resolution," *Journal of Physics D: Applied Physics*, vol. 54, p. 055201, feb 2021.

[35] N. Lepikhin, A. Klochko, N. Popov, and S. Starikovskaia, "Long-lived plasma and fast quenching of $N_2(C^3\Pi_u)$ by electrons in the afterglow of a nanosecond capillary discharge in nitrogen," *Plasma Sources Science and Technology*, vol. 25, no. 4, p. 045003, 2016.

[36] N. D. Lepikhin, N. A. Popov, and S. M. Starikovskaia, "Fast gas heating and radial distribution of active species in nanosecond capillary discharge in pure nitrogen and N_2:O_2 mixtures," *Plasma Sources Science and Technology*, vol. 27, no. 5, p. 55005, 2018.

[37] T. L. Chng, I. S. Orel, and S. M. Starikovskaia, "Electric field induced second harmonic (E-FISH) generation for characterization of fast ionization wave discharges at moderate and low pressures," *Plasma Sources Science and Technology*, vol. 28, no. 4, p. 045004, 2019.

[38] T. L. Chng, A. Brisset, P. Jeanney, S. M. Starikovskaia, I. V. Adamovich, and P. Tardiveau,

"Electric field evolution in a diffuse ionization wave nanosecond pulse discharge in atmospheric pressure air," *Plasma Sources Science and Technology*, vol. 28, p. 09LT02, sep 2019.

[39] A. Brisset, K. Gazeli, L. Magne, S. Pasquiers, P. Jeanney, E. Marode, and P. Tardiveau, "Modification of the electric field distribution in a diffuse streamer-induced discharge under extreme overvoltage," *Plasma Sources Science and Technology*, vol. 28, no. 5, p. 55016, 2019.

[40] Y. Zhu and S. M Starikovskaia, "Fast gas heating of nanosecond pulsed surface dielectric barrier discharge: Spatial distribution and fractional contribution from kinetics," *Plasma Sources Science and Technology*, vol. 27, p. 124007, 11 2018.

[41] X. Chen, Y. Zhu, and Y. Wu, "Modeling of streamer-to-spark transitions in the first pulse and the post discharge stage," *Plasma Sources Science and Technology*, vol. 29, no. 9, p. 095006, 2020.

[42] X. Chen, Y. Zhu, Y. Wu, J. Hao, X. Ma, and P. Lu, "Modeling of fast ionization waves in pure nitrogen at moderate pressure," *Plasma Sources Science and Technology*, feb 2021.

[43] N. Y. Babaeva and G. V. Naidis, "Simulation of subnanosecond streamers in atmospheric-pressure air: Effects of polarity of applied voltage pulse," *Physics of Plasmas*, vol. 23, no. 8, 2016.

[44] E. Marode, P. Dessante, and P. Tardiveau, "2D positive streamer modelling in NTP air under extreme pulse fronts. What about runaway electrons?," *Plasma Sources Science and Technology*, vol. 25, no. 6, p. 64004, 2016.

[45] A. Bourdon, F. ois Péchereau, F. Tholin, and Z. Bonaventura, "Study of the electric field in a diffuse nanosecond positive ionization wave generated in a pin-to-plane geometry in atmospheric pressure air," *Journal of Physics D: Applied Physics*, vol. 54, p. 075204, feb 2021.

[46] T. L. Chng, N. D. Lepikhin, I. S. Orel, and N. A. Popov, "TALIF measurements of atomic nitrogen in the afterglow of a nanosecond capillary discharge," *Plasma Sources Science and Technology*, vol. 29, no. 3, p. 35017, 2020.

[47] N. Popov, "Pulsed nanosecond discharge in air at high specific deposited energy: fast gas heating and active particle production," *Plasma Sources Science and Technology*, vol. 25, no. 4, p. 044003, 2016.

[48] A. V. Klochko, S. M. Starikovskaia, Z. Xiong, and M. J. Kushner, "Investigation of capillary nanosecond discharges in air at moderate pressure: comparison of experiments and 2D numerical modelling," *Journal of Physics D: Applied Physics*, vol. 47, no. 36, p. 365202, 2014.

[49] Y. Zhu, S. M. Starikovskaia, N. Y. Babaeva, and M. J. Kushner, "Scaling of pulsed nanosecond capillary plasmas at different specific energy deposition," *Plasma Sources Science and Technology*, vol. 29, p. 125006, dec 2020.

[50] S. A. Shcherbanev, C. Ding, S. M. Starikovskaia, and N. A. Popov, "Filamentary nanosecond surface dielectric barrier discharge. Plasma properties in the filaments," *Plasma Sources Science and Technology*, vol. 28, jun 2019.

[51] C. Ding, S. Shcherbanev, T. L. Chng, N. A. Popov, and S. Starikovskaia, "Streamer-to-Filamentary Transition and Electron Temperature Measurement in Positive Polarity Nanosecond Surface Discharge between 1 and 10 bar," in *AIAA Scitech 2019 Forum*, no. January, (Reston, Virginia), pp. 1–6, American Institute of Aeronautics and Astronautics, jan 2019.

[52] S. Stepanyan, A. Y. Starikovskiy, N. Popov, and S. Starikovskaia, "A nanosecond surface dielectric barrier discharge in air at high pressures and different polarities of applied pulses: transition to filamentary mode," *Plasma Sources Science and Technology*, vol. 23, no. 4, p. 045003, 2014.

[53] E. Anokhin, D. Kuzmenko, S. Kindysheva, V. Soloviev, and N. Aleksandrov, "Ignition of hydrocarbon: air mixtures by a nanosecond surface dielectric barrier discharge," *Plasma Sources Science and Technology*, vol. 24, no. 4, p. 045014, 2015.

[54] S. Shcherbanev, S. Stepanyan, N. Popov, and S. Starikovskaia, "Dielectric barrier discharge for multi-point plasma-assisted ignition at high pressures," *Phil. Trans. R. Soc. A*, vol. 373, no. 2048, p. 20140342, 2015.

[55] S. A. Shcherbanev, N. A. Popov, and S. M. Starikovskaia, "Ignition of high pressure lean H2:air mixtures along the multiple channels of nanosecond surface discharge," *Combustion and Flame*, vol. 176, pp. 272–284, 2017.

[56] S. A. Shcherbanev, A. Yu Khomenko, S. A. Stepanyan, N. A. Popov, and S. M. Starikovskaia, "Optical emission spectrum of filamentary nanosecond surface dielectric barrier discharge," *Plasma Sources Science and Technology*, vol. 26, no. 2, p. 02LT01, 2017.

[57] L. L. Alves, A. Bogaerts, V. Guerra, and M. M. Turner, "Foundations of modelling of nonequilibrium low-temperature plasmas," *Plasma Sources Science and Technology*, vol. 27, no. 2, 2018.

[58] G. J. M. Hagelaar and L. C. Pitchford, "Solving the Boltzmann equation to obtain electron transport coefficients and rate coefficients for fluid models," *Plasma Sources Science and Technology*, vol. 14, pp. 722–733, oct 2005.

[59] G. Naidis, "Effects of nonlocality on the dynamics of streamers in positive corona discharges," *Technical Physics Letters*, vol. 23, no. 6, pp. 493–494, 1997.

[60] N. Aleksandrov and I. Kochetov, "Electron rate coefficients in gases under non-uniform field and electron density conditions," *Journal of Physics D: Applied Physics*, vol. 29, no. 6, p. 1476, 1996.

[61] C. Li, W. Brok, U. Ebert, and J. Van der Mullen, "Deviations from the local field approximation in negative streamer heads," *Journal of applied physics*, vol. 101, no. 12, p. 123305, 2007.

[62] N. Liu and V. P. Pasko, "Effects of photoionization on propagation and branching of positive and negative streamers in sprites," *Journal of Geophysical Research: Space Physics*, vol. 109, p. A04301, 2004.

[63] G. K. Grubert, M. M. Becker, and D. Loffhagen, "Why the local-mean-energy approximation should be used in hydrodynamic plasma descriptions instead of the local-field approximation," *Physical Review E*, vol. 80, p. 036405, sep 2009.

[64] T. Piskin, V. A. Podolsky, S. O. Macheret, and J. Poggie, "Challenges in numerical simulation of nanosecond-pulse discharges," *Journal of Physics D: Applied Physics*, vol. 52, no. 30, p. 304002, 2019.

[65] V. Soloviev and V. Krivtsov, "Surface barrier discharge modelling for aerodynamic applications," *Journal of Physics D: Applied Physics*, vol. 42, no. 12, p. 125208, 2009.

[66] V. R. Soloviev, "Numerical modelling of nanosecond surface dielectric barrier discharge evolution in atmospheric air," *Plasma Sources Science and Technology*, vol. 27, no. 11, p. 114001, 2018.

[67] Y. Zhu, *Numerical Study of Nanosecond Capillary and Surface Dielectric Barrier Discharges : Kinetics , Transport and Fluid Responses*. PhD thesis, Ecole Polytechnique, 2018.

[68] V. R. Soloviev, V. M. Krivtsov, S. A. Shcherbanev, and S. M. Starikovskaia, "Evolution of nanosecond surface dielectric barrier discharge for negative polarity of a voltage pulse," *Plasma Sources Science and Technology*, vol. 26, p. 14001, 2017.

[69] C. Li, J. Teunissen, M. Nool, W. Hundsdorfer, and U. Ebert, "A comparison of 3d particle, fluid and hybrid simulations for negative streamers," *Plasma Sources Science and Technology*, vol. 21, no. 5, p. 055019, 2012.

[70] N. Y. Babaeva, C. Zhang, J. Qiu, X. Hou, V. F. Tarasenko, and T. Shao, "The role of fast electrons in diffuse discharge formation: Monte carlo simulation," *Plasma Sources Science and Technology*, vol. 26, no. 8, p. 085008, 2017.

[71] S. Pancheshnyi, M. Nudnova, and A. Starikovskii, "Development of a cathode-directed streamer discharge in air at different pressures: experiment and comparison with direct numerical simulation," *Physical Review E*, vol. 71, no. 1, p. 016407, 2005.

[72] P. Viegas, *Electric field characterization of atmospheric pressure Helium plasma jets through numerical simulations and comparisons with experiments*. PhD thesis, Ecole Polytechnique, 2018.

[73] A. Bourdon, V. Pasko, N. Liu, S. Célestin, P. Ségur, and E. Marode, "Efficient models for photoionization produced by non-thermal gas discharges in air based on radiative transfer and the Helmholtz equations," *Plasma Sources Science and Technology*, vol. 16, no. 3, pp. 656–678, 2007.

[74] A. Luque, U. Ebert, C. Montijn, and W. Hundsdorfer, "Photoionization in negative streamers: Fast computations and two propagation modes," *Applied Physics Letters*, vol. 90, no. 8, p. 081501,

2007.

[75] M. B. Zheleznyak, A. K. Mnatsakanian, and S. V. Sizykh, "Photoionization of nitrogen and oxygen mixtures by radiation from a gas discharge," *High Temperature Science*, vol. 20, pp. 423–428, nov 1982.

[76] S. Pancheshnyi, "Photoionization produced by low-current discharges in O_2, air, N_2 and CO_2," *Plasma Sources Science and Technology*, vol. 24, p. 015023, dec 2014.

[77] Y. Zhu, Y. Wu, and J. Li, "PHOTOPiC: Calculate photo-ionization functions and model coefficients for gas discharge simulations," https://arxiv.org/abs/2005.10021, 2020.

[78] S. Celestin, *Study of the dynamics of streamers in air at atmospheric pressure*. PhD thesis, Ecole Centrale Paris, 2008.

[79] S. Chen, J. C. Nobelen, and S. Nijdam, "A self-consistent model of ionic wind generation by negative corona discharges in air with experimental validation," *Plasma Sources Science and Technology*, vol. 26, no. 9, 2017.

[80] O. Eichwald, O. Ducasse, D. Dubois, A. Abahazem, N. Merbahi, M. Benhenni, and M. Yousfi, "Experimental analysis and modelling of positive streamer in air: towards an estimation of o and n radical production," *Journal of Physics D: Applied Physics*, vol. 41, p. 234002, nov 2008.

[81] L. W. Crispim, P. H. Hallak, M. S. Benilov, and M. Y. Ballester, "Modelling spark-plug discharge in dry air," *Combustion and Flame*, vol. 198, pp. 81–88, 2018.

[82] Y. Zhu, S. M. Starikovskaia, N. Y. Babaeva, and M. J. Kushner, "Scaling of pulsed nanosecond capillary plasmas at different specific energy deposition," *Plasma Sources Science and Technology*, vol. 29, p. 125006, dec 2020.

[83] F. Tholin and A. Bourdon, "Influence of temperature on the glow regime of a discharge in air at atmospheric pressure between two point electrodes," *Journal of Physics D: Applied Physics*, vol. 44, p. 385203, sep 2011.

[84] F. Tholin and A. Bourdon, "Simulation of the hydrodynamic expansion following a nanosecond pulsed spark discharge in air at atmospheric pressure," *Journal of Physics D: Applied Physics*, vol. 46, p. 365205, aug 2013.

[85] S. R. Sun, S. Kolev, H. X. Wang, and A. Bogaerts, "Coupled gas flow-plasma model for a gliding arc: investigations of the back-breakdown phenomenon and its effect on the gliding arc characteristics," *Plasma Sources Science and Technology*, vol. 26, p. 015003, nov 2016.

[86] S. Kolev and A. Bogaerts, "A 2d model for a gliding arc discharge," *Plasma Sources Science and Technology*, vol. 24, p. 015025, dec 2014.

[87] S. R. Sun, S. Kolev, H. X. Wang, and A. Bogaerts, "Investigations of discharge and post-discharge in a gliding arc: a 3d computational study," *Plasma Sources Science and Technology*, vol. 26, p. 055017, apr 2017.

[88] P. Tardiveau, N. Moreau, S. Bentaleb, C. Postel, and S. Pasquiers, "Diffuse mode and diffuse-to-filamentary transition in a high pressure nanosecond scale corona discharge under high voltage," *Journal of Physics D: Applied Physics*, vol. 42, no. 17, p. 175202, 2009.

[89] V. F. Tarasenko, G. V. Naidis, D. V. Beloplotov, I. D. Kostyrya, and N. Y. Babaeva, "Formation of Wide Streamers during a Subnanosecond Discharge in Atmospheric-Pressure Air," *Plasma Physics Reports*, vol. 44, no. 8, pp. 746–753, 2018.

[90] A. Brisset, *Physics of nanosecond diffuse discharges under very high electric fields (in French)*. PhD thesis, l'Université Paris-Saclay, 2019.

[91] Y. Zhu and Y. Wu, "The secondary ionization wave and characteristic map of surface discharge plasma in a wide time scale," *New Journal of Physics*, vol. 22, no. 10, p. 103060, 2020.

[92] J. Teunissen, A. Sun, and U. Ebert, "A time scale for electrical screening in pulsed gas discharges," *Journal of Physics D: Applied Physics*, vol. 47, no. 36, p. 365203, 2014.

[93] A. Brisset, K. Gazeli, L. Magne, S. Pasquiers, P. Jeanney, E. Marode, and P. Tardiveau, "Modification of the electric field distribution in a diffuse streamer-induced discharge under extreme overvoltage," *Plasma Sources Science and Technology*, vol. 28, p. 055016, may 2019.

[94] Y. S. Akishev, V. Karalnik, M. Medvedev, A. Petryakov, T. Shao, C. Zhang, and B. Huang, "About

the possible source of seed electrons initiating the very first breakdown in a DBD operating with the air at atmospheric pressure," *Plasma Sources Science and Technology*, vol. 29, p. 465705, jan 2021.

[95] V. I. Gibalov and G. J. Pietsch, "The development of dielectric barrier discharges in gas gaps and on surfaces," *Journal of Physics D: Applied Physics*, vol. 33, pp. 2618–2636, oct 2000.

[96] D. Braun, V. Gibalov, and G. Pietsch, "Two-dimensional modelling of the dielectric barrier discharge in air," *Plasma Sources Science and Technology*, vol. 1, pp. 166–174, aug 1992.